BIRZEIT UNIVERSITY

FACULTY OF GRADUATE STUDIES

A Comparative Study of Fe Nanoparticles and Bimetallic Fe-Ni Nanoparticles in the Removal of Bromophenol Blue from Aqueous Solutions

دراسة مقارنة بين دقائق الحديد النانوية والدقائق النانوية المختلطة للحديد والنيكل في إزالة مادة "بروموفينول بلو" من المحاليل المائية

This Thesis was submitted in partial fulfillment of the requirements for the

Master's Degree in Applied Chemistry

From the Faculty of Graduate Studies at Birzeit University, Palestine

By: Raheeq Naser

Supervised by: Prof. Talal Shahwan

June 2018

A Comparative Study of Fe Nanoparticles and Bimetallic Fe-Ni Nanoparticles in the Removal of Bromophenol Blue from Aqueous Solutions

By

Raheeq Naser

This thesis was prepared under the supervision of Prof. Talal Shahwan and has been approved by all members of the Examination Committee:

Examination Committee:

Prof. Talal Shahwan

Supervisor _____ .

Dr. Saleh Sulaiman

Committee Member _____.

Dr. Mohammed Aljabari

Committee Member _____.

Date of Defense: 21-06-2018

Acknowledgement

I am very grateful to God for being with me every second of my life until I have reached what I am now.

I would like to express my thanks and gratitude to the supervisor on my thesis, Prof. Talal Shahwan for his full and continuous support on all levels, his office door was always open whenever I ran into a trouble spot or had a question about my research or thesis writing. Thank you for being patient, for your motivation and for all that you have taught me …

I would like also to thank the members of the thesis committee, Dr. Saleh Sulaiman & Dr. Mohammed Aljabari for their efforts in reading and assessing.

I would like to thank all the professors in the department of chemistry and laboratory technicians Mr. I. Shalash, Mr. A. Mubarak, and Mr. A. Doudin.

Great thanks and appreciation to prof. Armin Gölzhäuser and his group at Bielefeld University –Germany, especially Miss Yang Yang for her help in XPS analysis.

And of course many thanks to Mrs. Montaha Masri at Ulm University- Germany who helped in SEM, TEM and XRD characterizations.

Finally yet importantly, I must express my very profound gratitude to my parents and to my brothers and sisters, for their support and encouragement throughout the years.

Abstract

Water pollution is the most global problem in the 21st century and it has many aspects and causes different impacts. The problem is caused mainly by human activities, such as industry. Textile industry is one of the huge wastewater sources as recorded by the Central Pollution Control. The textile effluents are very complex and difficult to treat. It contains pollutants that differ in the chemical and physical properties, suspended materials, and non-biodegradable compounds such as detergent, dyes and fibers.

During the last two decades, iron-based nanomaterials were globally widely investigated due to its high removal capacity toward a wide range of water pollutants. Iron-based bimetallic nanoparticles are being studied as an alternative to pure iron nanoparticles, in order to enhance the reactivity of the material.

In this research, iron nanoparticles (Fe NPs) and bimetallic iron-nickel nanoparticles (Fe-Ni NPs) were synthesized by co-liquid phase reduction method and characterized using XRD, XPS, SEM and TEM techniques.

A comparative study was performed to assess the efficiency of Fe and Fe-Ni NPs in the removal of bromophenol blue (BPB) dye from water.

The effect of various parameters on the removal process was inspected, such as sample composition, time, initial dye concentration, pH, and temperature.

The results of the experiments showed that the efficiency of Fe NPs towards dye removal was higher than that of Fe-Ni NPs. Moreover, the dye removal process using Fe NPs was much faster than of Fe-Ni NPs. The kinetics data showed that the removal of BPB by Fe and Fe-Ni NPs follow pseudo-second order rate equation. The effect of initial dye concentration data were used to evaluate “apparent equilibrium constant (K)” values over a concentration range of 20-100 mg/L, based on a modified form of the linear isotherm.

For both types of NPs, the removal extent of dye decreased as the temperature increased, indicating exothermic behavior. Entropy of the system decreased in both cases, and the pH had minimal effects on the removal of the dye by both types of nanomaterials.

ملخص الدراسة

تلوث المياه هو المشكلة الأكثر عالمية في القرن الواحد والعشرين، وله أشكال عديدة ويسبب تأثيرات مختلفة. هذا التلوث هو نتاج للأنشطة البشرية الصناعية مثل صناعة الغزل والنسيج والتي تعد واحدة من أكبر مصادر تلوث المياه كما سجلها "مركز السيطرة على التلوث". المياه الملوثة الصادرة عن الصناعات النسيجية معقدة التركيب وصعبة المعالجة وذلك نظراً لاحتوائها على ملوثات تختلف في الخواص الكيميائية والفيزيائية ومواد ذائبة ومركبات غير قابلة للتحلل البيولوجي مثل المنظفات والصبغات والألياف النسيجية.

من بين الطرق المستخدمة لمعالجة المياه الملوثة، جذب انتباه الباحثون طريقة الادمصاص خاصة باستخدام دقائق الحديد النانوية بسبب قدرته العالية على إزالة مجموعة واسعة من ملوثات المياه. يواجه استخدام دقائق الحديد النانوية تضاؤل التفاعل مع مرور الوقت بسبب الأكاسيد التي تتشكل على الطبقة الخارجية. تم اقتراح طريقة موثقة بشكل جيد وهي تحضير الجسيمات النانوية ثنائية المعدن (سبيكة) لزيادة التفاعل.

في هذا البحث، تم تحضير دقائق الحديد النانوية، وخليط من دقائق الحديد والنيكل النانوية(ثنائية المعدن) الأشعة بواسطة طريقة الاختزال المشترك في الحالة السائلة وتم تشخيص العينات باستخدام تقنيات عدة.

أُجريت دراسة مقارنة بين كفاءة كل من دقائق الحديد ودقائق الحديد والنيكل النانوية ثنائية المعدن في إزالة صبغة "البروموفينول بلو" من الماء.

خلال الدراسة، تم فحص تأثير العوامل المختلفة على عملية الإزالة مثل تركيبة العينة، والوقت، التركيز الأولي للصبغة، درجة الحموضة ودرجة الحرارة.

أظهرت نتائج التجارب أن كفاءة إزالة دقائق الحديد النانوية كانت أعلى من الحديد والنيكل النانوية ثنائية المعدن. علاوة على ذلك، كانت عملية الإزالة أسرع بكثير في حالة استخدام دقائق الحديد النانوية منه في حالة دقائق الحديد والنيكل النانوية ثنائية المعدن.

كما أظهرت دراسة سرعة التفاعل أن إزالة صبغة "البروموفينول بلو" باستخدام دقائق الحديد النانوية و دقائق الحديد والنيكل النانوية تتبع معدل تغير من الدرجة الثانية.

استخدم تأثير التركيز الأولي للصبغة من أجل احتساب ثوابت اتزان ضمن التراكيز من (20-100) ملغم/لتر وذلك باستخدام معادلة خطية معدّلة.

أظهرت الدراسة كذلك أن إزالة صبغة "البروموفينول بلو" يقل معدلها مع ازدياد درجة الحرارة وهذا يشير إلى أن التفاعل طارد للحرارة. لوحظ أن انتروبيا النظام قد تناقصت في كلتي الحالتين، وأن الرقم الهيدروجيني لم يكن له تأثير ملحوظ على إزالة الصبغة باستخدام المادتين النانويتين.

Table of Contents

Acknowledgement I

Abstract II

ملخص الدراسة IV

List of Figures VIII

List of Tables IX

List of Abbreviations X

Chapter 1: INTRODUCTION 1

1.1 Water Pollution and Iron Nanotechnology 1

1.2 Iron-Based Bimetallic Nanoparticles 7

1.3 Dyes Pollution 13

1.4 Study Purpose 17

Chapter 2: EXPERIMENTAL 18

2.1 Chemicals and Reagents 18

2.2 Synthesis of Iron and Iron-Nickel Bimetallic Nanoparticles 18

2.2.1 Synthesis of Iron Nanoparticles (Fe NPs) 19

2.2.2 Synthesis of Iron Nickel Bimetallic Nanoparticles 20

2.3 Dye Removal Experiments 21

2.3.1 Dye Removal Kinetics 22

2.3.2 Effect of Initial Dye Concentration 23

2.3.3 Effect of pH 23

2.4 Characterization Techniques 24

2.4.1 Ultraviolet-Visible (UV-Vis) Spectrophotometry 24

2.4.2 Powder X-Ray Diffraction (XRD) 25

2.4.3 Scanning Electron Microscopy (SEM) 25

2.4.4 Transmission Electron Microscopy (TEM) 26

2.4.5 X-Ray Photoelectron Spectroscopy (XPS) 26

Chapter 3: RESULTS & DISCUSSION 28

3.1 Characterization the Synthesized Nanoparticles Materials 28

3.1.1 Characterization of Fe NPs 28

3.1.2 Iron - Nickel Bimetallic Nanoparticles (Fe-Ni) NPs 33

3.2 Effect of Sample Composition on the Removal Percentage of BPB 38

3.3 Dye Removal Kinetics 40

3.4 Effect of Initial Dye Concentration 56
3.5 Effect of Temperature: 61
3.6 Effect of pH on the Removal of BPB 65
3.7 Degradation Products Analysis 66
4. Conclusions 67
5. References 68

List of Figures

Figure 1.1 The core-shell model of zero-valent iron nanoparticles.[15] 5
Figure 1.2 Mechanism of hydrodechlorination on the surface of 11
Figure 1.3 Bromophenol blue structure 15

Figure 2.1 The calibration curve of bromophenol blue 25

Figure 3.1 XRD pattern showing the basic reflections of Fe NPs 28
Figure 3.2 SEM images of Fe NPs at two different magnifications 29
Figure 3.3 TEM images of Fe NPs at two different magnifications 30
Figure 3.4 XPS spectrum for a sample of Fe NPs 31
Figure 3.5 XPS features of Fe 2p in Fe NPs 32
Figure 3.6 XRD pattern for Fe-Ni (4:1)S bimetallic nanoparticle 33
Figure 3.7 SEM (a,b) and TEM (c,d) images of Fe-Ni bimetallic nanoparticles 34
Figure 3.8 HIM analysis of Fe-Ni bimetallic nanoparticles 35
Figure 3.9 XPS analysis for (4:1)S Fe-Ni bimetallic NPs 36
Figure 3.10 XPS features of Fe 2p in Fe-Ni NPs (4:1)S sample 37
Figure 3.11 XPS features of Ni 2p in Fe-Ni NPs (4:1)S sample 37
Figure 3.12 Effect of Ni content in Fe-Ni NPs on the removal % of BPB 38
Figure 3.13 Effect of iron source on the removal % 39
Figure 3.14 Effect of Fe NPs mass on the removal percentage of BPB 40
Figure 3.15 Variation of dye concentration with time: (a) for Fe and Fe-Ni NPs, (b) for Ni NPs 42
Figure 3.16 Pseudo second order linear fits for the removal of BPB by: (a) Fe NPs (b) Fe-Ni NPs. 45
Figure 3.17 Nonlinear fits of the kinetic data of BPB removal by Fe NPs; (a) using Shahwan equation (b) using Ho equation. 48
Figure 3.18 Nonlinear fits of the kinetic data of BPB removal by Fe-Ni NPs; (a) using Shahwan equation (b) using Ho equation. 48
Figure 3.19 Pseudo first order linear fit for Ni NPs using original Lagergren equation and modified Lagergren equation 52
Figure 3.20 Nonlinear fits of the kinetic data of BPB removal by Ni NPs; (a) using Lagergren equation (b) using modified Lagergren equation. 54
Figure 3.21 Variation of Q with C_0 for BPB using three different NPs types: Fe NPs, Fe-Ni NPs (1:1) S and Fe-Ni NPs (4:1) S. 59
Figure 3.22 Variation of Q with C_0 for BPB removal by: (a) Fe NPs, (b) Fe-Ni NPs at 323 K 63
Figure 3.23 UV-Vis spectra of BPB before and after treatment with Fe NPs. 66

List of Tables

Table 1.1 Standard electrode reduction potential values of some metals in aqueous solution at 25˚C.[26] 7

Table 2.1 Amount of Iron and Nickel salts used to prepare Fe-Ni NPs 20
Table 2.2 Amount of KHP or KH_2PO_4, HCl and NaOH used to prepare adjusted buffers at specific pH 24

Table 3.1 Variation of the BPB concentration (mg/L) with different contact times for Fe and Fe-Ni NPs. 41
Table 3.2 Kinetic constants for BPB onto Fe and Fe-Ni NPs by linear regression analysis method 46
Table 3.3 Values of Q obtained from experiment, values of Q_m predicted by Shahwan model, values of Q_e predicted by Ho model, and the Chi-test values for the two sorption systems. 50
Table 3.4 Kinetic constants for BPB removal by Ni NPs. 53
Table 3.5 values of k and Q_m for the three sorption systems 55
Table 3.6 The calculated Q values of BPB on three different NPs types at various BPB initial concentrations. 58
Table 3.7 Values of coefficient of determination (R^2), K`, K, and ΔG˚ obtained for sorption of BPB on three different NPs types at 298 K. 60
Table 3.8 Values of Q obtained for sorption of BPB on Fe and Fe-Ni at 298 K and 323 K using different initial dye concentrations. 62
Table 3.9 The values of ΔH˚, ΔG˚ and ΔS˚ associated with removal of BPB from solutions at temperatures of 298 and 323K. 65

List of Abbreviations

BPB	Bromophenol Blue dye
Fe NPs	Iron nanoparticles
Fe-Ni NPs	Iron nickel bimetallic nanoparticles
nZVI	Zero valent Iron nanoparticles
Ni NPs	Nickel nanoparticles

Chapter 1: INTRODUCTION

1.1Water Pollution and Iron Nanotechnology

Environmental pollution is one of the most important issues around the world nowadays. Pollution is rapidly increasing and threatening the main components in our environment; water, air and soil.[1] Water is among the most crucial needs in life. It forms about 55% to 70% of human body and covers about 70% of the Earth's surface, whilst only 0.002% of the water is safe for human consumption.[2] Moreover, energy production, economic development and global health are inextricably linked to the availability of safe water.[3] At the same time, the access to safe water is the major global challenge for the 21st century mainly due to human activities, which lead to contamination of the water sources.[4,5]

Lack of fresh and safe water is associated with many problems. Around 1.2 billion people do not have access to clean drinking water, millions of people die annually from diseases transmitted through unsafe water.[6]

There are three sources of water pollution sorted as; natural sources, industrial wastes and domestic sources. Natural sources include thermal and acid effluents from volcanic areas. Industrial wastes include chemical plants, mining facilities, and textile mills, which contain high amounts of toxic chemical specie.

Domestic sources include laundry wastes and sewage, and the treatment of the wastewater is often very complicated because it contains mixtures of various pollutants.[2]

A remediation process refers to removal, minimization, or neutralization of the contaminants, which exist in water and can damage human health or ecosystems. Remediation technologies can be divided into three categories: (1) thermal, (2) physicochemical and (3) biological methods.[1]

Thermal water treatment is based mainly on heating, in order to sterilize and/or separate components.[7] In physiochemical methods, the treatment usually includes physical processes like adsorption or filtration followed by chemical methods such as oxidation, photochemical methods, or electrochemical degradation.[8,9] Biological methods refer to using microorganisms such as bacteria and fungal in dye removal or in aerobic or anaerobic degradation.[10,11]

Most traditional methods such as extraction, adsorption and oxidation are less effective, expensive, and time-consuming. Whereas, biological degradation is more environmental friendly and inexpensive, but it is very time-consuming.[1,12]

Among diverse physiochemical and biological wastewater treatment processes, nanotechnology can effectively contribute to wastewater treatment. This is

conveyed by virtue of special characteristics such as large surface to volume ratio, high affinity, reuse, high capacity and selectivity for heavy metals and other contaminants.[13,14]

As particle size decreases, the proportion of surface atoms increases, leading to a stronger tendency of surface atoms to interact, adsorb, and react with foreign atoms or molecules in order to achieve surface stabilization.[15,16]

On the overall, nanotechnology has a great potential to improve the quality of the environmental components (water, soil, and air). There are three major applications of nanotechnology which can be classified as[1,17];

(i) Restoration (or remediation) and purification of contaminated material,

(ii) Pollution sensing and detection,

(iii) Pollution prevention by applying material technology.

Nano zero valent iron (nZVI) is one of the products of environmental nanotechnology that has been widely investigated during the last two decades. This material has been shown to be very effective towards a wide spectrum of pollutants such as organic dyes, chlorinated organic compounds and heavy metals.[18]

The efficiency of nZVI is mainly due to its low oxidation-reduction potential, very high surface area, and small particle size. Moreover, it has been widely inspected as an environmental friendly material .[19- 21]

It has been shown that individual nZVI particles has a spherical shape, with a core-shell structure (see Fig.1.1). The shell is typically composed of iron (hydro)oxide layers with a thickness of several nanometers. On the other hand, the core is composed of metallic iron Fe(0). By virtue of its structure, nZVI can act as a reductant via the Fe(0) core, or as a sorbent via the iron ((hydro)oxide shell. nZVI can also serve as a coagulant for various anions in groundwater through the dissolution of Fe(II) from the nZVI surface. The interfacial reactions of nZVI (dissolution, adsorption, redox reaction, and precipitation) can occur simultaneously or sequentially on the surface of nZVI during the decontamination process.[22]

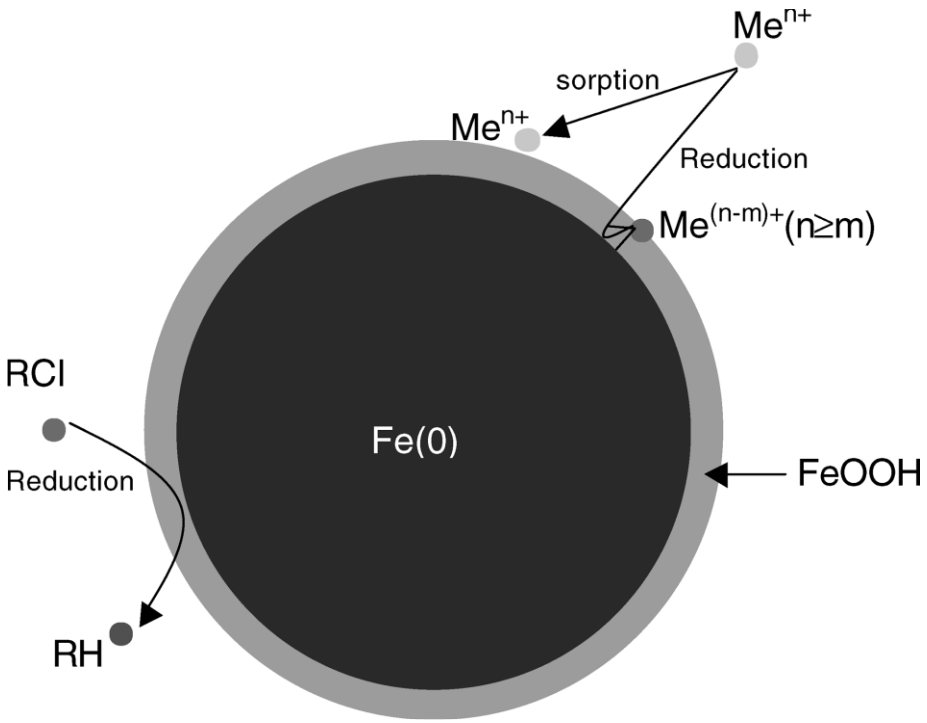

Figure 1.1 The core-shell model of zero-valent iron nanoparticles.[15]

Thus, the mechanistic details of contaminant removal by nZVI might be complex and dynamic. The removal process can also be affected by structural transformation of nZVI. During contaminant removal, the nZVI particle transformations can be classified into two categories: accretion on nZVI surface due to the formation of hydroxide, or coprecipitation and corrosion of nZVI core due to reactions with contaminants, water, oxygen and other oxidants.[19]

There are many applications on the usage of nZVI in wastewater treatment. One of the famous field applications started in 1990 and involved using permeable reactive barrier (PRB) for treating water in the aquifer without pumping water out to the

surface and reinjecting it back to the acquifer, as it is the case in traditional pump-and-treat technology. In a PRB structure, groundwater flows through an engineered iron wall while contaminants are reduced, adsorbed, or transformed in contact with the nZVI surface.[23]

In addition, magnetic nanoparticles have applications in biomedical fields, which include directed drug delivery, the labeling and magnetic separation of biological materials, and hyperthermia treatment.[11]

1.2 Iron-Based Bimetallic Nanoparticles

Bimetallic nanoparticles consist of two different metal elements synthesized with nano size. Within the bimetallic complex, one metal (for example Fe, Zn) behaves as electron donor while the other might behave as catalyst (Pd, Pt). The combinations are selected based on their standard reduction potentials (Table 1.1), with the second metal being electropositive relative to the primary metal. Adding the second metal lead to improve of the catalytic properties of the original single metal.[24,25]

Table 1.1 Standard electrode reduction potential values of some metals in aqueous solution at 25°C.[26]

Metal	Half reaction	Standard electrode potential (E°), V
Fe	$Fe_2^+ + 2e \Leftrightarrow Fe$	-0.44
Ni	$Ni_2^+ + 2e \Leftrightarrow Ni$	-0.257
Si	$SiO_2 + 4H^+ + 4e \Leftrightarrow Si + 2H_2O$	-0.909
Al	$Al_3^+ + 3e \Leftrightarrow Al$	-1.676
Zn	$Zn_2^+ + 2e \Leftrightarrow Zn$	-0.763
Mg	$Mg_2^+ + 2e \Leftrightarrow Mg$	-2.356
Pd	$Pd_2^+ + 2e \Leftrightarrow Pd$	0.915
Pt	$Pt_2^+ + 2e \Leftrightarrow Pt$	1.188
Cu	$Cu_2^+ + 2e \Leftrightarrow Cu$	0.34

Various methods has been used to prepare bimetallic nanoparticles, those include:

(1) Physically mixing: the nanoparticles prepared separately from the primary metal (for example ZVI) and the secondary metal (Ni) at specific weight ratios.[27,28]

(2) Co-liquid phase reduction: where the salts of the two metals are mixed together then the reducing agent is added to the solution.[29]

(3) Post deposition of the second metal on the surface of the primary metal particles.[30,31]

A new generation of bimetallic nanoparticles has been synthesized. It consists of iron as a base metal that behaves as a reductant doped with another metal such as palladium, platinum or nickel which behave as a catalyst.

These nanoparticles could have higher reaction rate compared with the monometallic nanoparticles.[32] Bimetallic nanoparticles are reported to exhibit ability to reduce various types of organic pollutants such as (organic dyes, chlorinated alkanes, alkenes and aromatic, pesticides) and inorganic anions (nitrates) in aqueous solutions to less toxic byproducts.[33]

These nanoparticles were used in the treatment of chlorinated organic compounds because it is very fast and have ability to degrade these type of contaminants completely.[34] The presence of a second metal lowers the activation energy and increases the rate of dechlorination reactions.[25] In addition, it is reported to create novel catalytic properties that are absent in the monometallic particles and enhance chemical reactivity by changing the electronic properties of the surface.[35]

The search for bimetallic nanoparticles is motivated by a number of limitations and obstacles in the application of mono iron NPs technology for the treatment of contaminated water. In the treatment of chlorinated organic compounds, for example, toxic byproducts can be produced and accumulated due to the low reactivity of nZVI towards these compounds.[25,36] In addition, iron reactivity decrease over time, due to the changes in the iron surface morphology resulted from the formation of isolated shell layer consisting of iron oxides, -hydroxides, or –carbonates. [31,37-39]

In bimetallic nanoparticles, iron leads to the hydrogen gas generation by corrosion reactions in water, and the second metal acts as a hydrogenation catalyst which is necessary for the degradation step.[34] The hydrogen generation reaction is represented by:

$$Fe^0 + 2H^+ \rightarrow Fe^{2+} + H_2$$

The electrons and the generated hydrogen are utilized by a second dopant metal to catalyze the reaction through the formation of active surface metal-hydride as a powerful reductant represented as:

$$2M + H_2 \rightarrow 2M{-}H$$

Where M can be nickel or palladium.[32,40,41]

Dechlorination of pollutants is one of the most widely studied reactions using iron-based nanomaterials, which was used to shed light on the mechanisms of degradation of organic pollutants. Two mechanisms have been proposed for the dechlorination reactions by using zero-valent metals:

(1) Reduction of chlorinated organic molecule adsorbed on the metal surface by direct transfer of electrons from the metal to the surface, leading to the release of chloride ions and formation of hydrocarbons.

(2) Catalytic hydro-dehalogenation when the bimetallic NPs are used, which includes hydrogenation of the chlorinated organics with adsorbed hydrogen produced during metal corrosion by water, as shown in Fig. 1.2.[29,40,42,43]

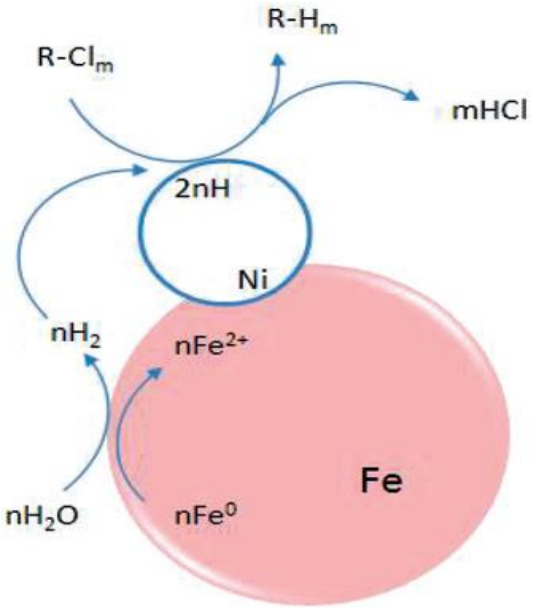

Figure 1.2 Mechanism of hydrodechlorination on the surface of Fe–Ni nanoparticles[40]

Most of the published research about bimetallic nanoparticles have focused on the degradation of chlorinated organic compounds, while few research has been done on dye removal.

Fe-Ni nanoparticles have been used in the degradation of azo dye orange G. The reaction is reported to result in complete degradation of the dye after 10 minutes, and the proposed mechanism suggests the cleavage of azo linkage.[44]

The dechlorination of halogenated organic compounds using Fe-Ni NPs is reported to overpass the effectivity of other bimetallic NPs. According to the same study, this was achieved without producing dangerous chlorinated intermediates, and can

be applied in situ by embedding the bimetallic Fe/Ni NPs in a membrane to prevent dissolution of nickel into the media.[45]

The catalytic properties of nickel are thought to stimulate the formation of atomic hydrogen or hydride on the surface, and enhance the electronic properties of the iron, thus expediting the reductive pathways of the dechlorination reactions.[46]

1.3 Dyes Pollution

The global textile and clothing industry is very huge, it forms the second basic requirement of humans.[47]

The textile dyeing industry consumes large amounts of water and consequently produces large volumes of wastewater, which is often rich in colors and contains residues of reactive dyes. The dyes are mainly aromatic and heterocyclic compounds, and have color display groups which are known as chromophores and polar groups. Their structure is usually not that simple and stable; as a result their degradation is very difficult. [48,49]

It is estimated that more than 10000 different types of dyes are used in the textile industry. In addition, over $7x\ 10^5$ tons of dyes are synthesized annually around the world.[50]

Dyes can cause allergic reactions, and can be carcinogenic, and mutagenic. For example, it has been reported that exposure to azo dyes in contaminated water for a long time cause some types of cancer, like bladder, after using. Azo dyes are metabolized in the liver and at the intestinal wall, and produce free aromatic amines that are carcinogenic and mutagenic.[51-53]

There are various types of dyes, which can be classified according to different parameters such as solubility, charge and application field. For example, dyes could be ionic, cationic or nonionic according to the net charge on their structure. Many dye types are sorted as soluble like acid, basic, mordant, metal complex, direct and reactive dyes, while insoluble dyes include azoic, sulfur, vat and disperse dyes.[8]

In accordance with that, many methods can be applied to remove dyes from wastewater, like electrochemical coagulation, reverse osmosis, nano filtration, adsorption using activated materials etc.[55] The major limitation to those methods is that the wastewater usually contains a lot of dyes which differ in the chemical and physical properties, and the applied removal method could usually be suitable for only one or two types of dyes.[54,56,57]

In this study, we will focus on “Bromophenol Blue” as a model of dyes pollutant, which is an acid dye, used as a color mark to monitor the process of agarose gel electrophoresis and polyacrylamide gel electrophoresis, coloring proteins in paper electrophoresis and is also a pH indicator. This dye is widely used as an industrial dye for foods, drugs, cosmetics, textiles, printing inks and laboratory indicators[58] . The structure of the dye is shown in Fig. 1.3.[59]

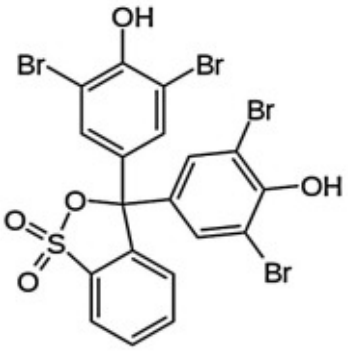

Figure 1.3 Bromophenol blue structure

Different studies are reported in literature about the removal of aqueous bromophenol blue.

One of those studies is the oxidation of bromophenol blue, using potassium dichromate, oxalic acid and sodium carbonate. The temperature of the mixture was adjusted at 30°C using a thermostat, then aliquots of the mixture were withdrawn at different times, and the absorbance was recorded at 590 nm. The color was removed completely, but the main disadvantage of this method is the releasing of chromium ions Cr(III) and Cr(VI) into the solution.[58]

Bromophenol blue was removed from water using activated charcoal as adsorbent material. The adsorption efficiency was observed to decrease as the pH and temperature increase, and the thermodynamic parameters values were reported.[59]

The removal of bromophenol blue using α-chitin nanoparticles was studied by Dhananasekaran et al.[60] Chitin is a biopolymer, found in arthropod cuticle include the crustaceans, arachnids, insects and centipedes. The removal percentage was 79%, but the preparation of the chitin to be used as an adsorbent takes around one month.

In another study, a polymer clay composite consisting of kaolinite clay crosslinked with polyacrylamide co-acrylic was used as an adsorbent material. The removal efficiency of the adsorbant towards bromophenol blue was 95%.[61]

Photocatalysis have been used for the removal of bromophenol blue. For example, it is reported that TiO_2 could be used to decolorized bromophenol blue under UV irradiation. Complete decolrization was achieved after 70-100 minutes irradiation in a natural solution (pH=6.3) at 20 ˚C.[62]

Certain types of nanomaterials are reported in literature as possible choices for the removal of bromophenol blue such as Fe_2O_3–ZnO–$ZnFe_2O_4$/C nanocomposite and CuO-nano-clinoptilolite.[63,64] Fe_2O_3–ZnO–$ZnFe_2O_4$/C nanocomposite was applied with an ultrasound assisted method. Decolorization is reported to reach maximum adsorption capacity of 90.91mg/g. On the other hand, CuO-NCP composite was used for the photodeclorization, and the declorization extent was 32% after 180 minutes of irradiation time.

1.4 Study Purpose

This study focuses on the synthesis of iron nanoparticles (Fe NPs), and bimetallic iron-nickel nanoparticles (Fe-Ni NPs) at various Fe/Ni ratios, and then using these materials in removal of bromophenol blue from aqueous solution. The prepared materials were characterized using Scanning Electron Microscopy (SEM) and Transmission Electron Microscopy (TEM) to investigate and compare their nanoscale morphology. X-Ray powder Diffraction (XRD) was used to determine the mineralogical structure of the materials. X-Ray Photoelectron Spectroscopy (XPS) was employed to determine the quantitative elemental surface composition and the oxidation states of the surface species. The dye concentration was monitored using UV-visible spectrophotometry.

The prepared materials were separately used in the removal of bromophenol blue on a comparative basis. Experimental parameters such as iron to nickel ratio, dye initial concentration, temperature, pH and contact times were investigated.

Chapter 2: EXPERIMENTAL

2.1 Chemicals and Reagents

Throughout this study the following chemicals were used without further purification; Iron (II) chloride tetrahydrate, $FeCl_2.4H_2O$, (Aldrich 22029-9), Ferrous sulfate heptahydrate $FeSO_4.7H_2O$ (Aldrich 7782-63), Nickel chloride hexahydrate $NiCl_2.6H_2O$ (Aldrich 7791-20), Sodium borohydride, $NaBH_4$, (Merck 8.06373), absolute Ethanol (J.T. Baker 8006), Bromophenol blue $C_{19}H_{10}Br_4O_5S$ (95%) (Aldrich 61698), Potassium dihydrogen phosphate KH_2PO_4 (Aldrich 45369) and Potassium hydrogen phthalate $C_8H_5KO_4$ (Merck 545-K764274). All aqueous solutions were prepared using deionized water.

2.2 Synthesis of Iron and Iron-Nickel Bimetallic Nanoparticles

Iron nanoparticles and Iron-Nickel bimetallic nanoparticles were prepared using liquid phase reduction method with borohydride ions as the reducing agent, in accordance with procedures reported in several previous publications.[29,31,65]

2.2.1 Synthesis of Iron Nanoparticles (Fe NPs)

For each batch, 5.34 g of $FeCl_2.4H_2O$ was dissolved in 25.0 mL 4:1 (ethanol: water) solution and kept under magnetic stirring conditions for 15 min. The $NaBH_4$ solution was prepared separately by dissolving 2.54 g in 70.0 mL of water.

Then, borohydride solution was added to the iron salt solution using a burette at a constant addition rate of about 0.5 mL sec^{-1} under continuous magnetic stirring conditions. During the addition of the borohydride solution, the iron solution color converted from brown to black and H_2 gas evolution was observed and a sharp rise in pH was observed, indicating a successful reduction of Fe^{2+} to Fe^0 according to the following chemical equation:

$$Fe^{2+} + 2BH_4^- + 6H_2O \rightarrow Fe^0 + 2B(OH)_3 + 7H_{2(g)} \uparrow$$

The solution of Fe NPs was kept under stirring conditions for another 15 min, after completing the addition of the borohydride solution. Vacuum filtration was used to separate the produced Fe NPs, and while still on suction filter, the black Fe NPs powder was washed with absolute ethanol three times. Finally, Fe NPs sample was dried in the oven at 90°C for 6 hours.

2.2.2 Synthesis of Iron Nickel Bimetallic Nanoparticles

Two types of iron salt were used to synthesize bimetallic (Fe-Ni) nanoparticles which are Iron (II) chloride tetrahydrate, $FeCl_2.4H_2O$, and Iron(II) sulfate heptahydrate ($FeSO_4.7H_2O$).

The procedure was the same as used for Fe NPs except that different amounts of iron and nickel were mixed and kept under continuous stirring for 15 min., before adding the borohydride solution. The amount of each salt varied depending on the molar ratio between Iron and Nickel, and the quantities used are given in Table 2.1:

Table 2.1 Amount of Iron and Nickel salts used to prepare Fe-Ni NPs

	Iron salt mass	Nickel salt mass	Symbol (Fe:Ni)
Sample 1	3.0750g $FeSO_4.7H_2O$	0.7500g $NiCl_2.6H_2O$	(4:1) S
Sample 2	3.0558g $FeSO_4.7H_2O$	2.6147g$NiCl_2.6H_2O$	(1:1) S
Sample 3	2.1870g $FeCl_2.4H_2O$	2.6150g $NiCl_2.6H_2O$	(1:1) Cl
Sample 4	1.0940g $FeCl_2.4H_2O$	2.6150g $NiCl_2.6H_2O$	(1:2) Cl
Sample 5	1.0940g $FeCl_2.4H_2O$	5.2290g $NiCl_2.6H_2O$	(1:4) Cl

'S' symbol indicates Iron (II) sulfate salt, 'Cl' symbol indicates Iron (II) chloride salt

2.3 Dye Removal Experiments

Through this study, all of the solutions were prepared in potassium hydrogen phthalate (KHP) buffer solution (pH=4). This solution was prepared by dissolving 10.21g of KHP salt and 1ml of 0.1M HCl in 1.0L deionized water using a volumetric flask.[59]

A stock solution of Bromophenol blue (BPB) at a concentration of 100 mg/L was prepared by dissolving exactly 263.0 mg dye in 250 ml KHP buffer solution (pH=4). Further analytical dilutions were made when needed using volumetric pipettes.

Calibration curve in the range of 1.0-10.0 mg/L for BPB where constructed immediately after the preparation of the stock solutions. The calibration curve was obtained by measuring the UV-Visible absorbance at λmax (590 nm) of the dye using Varian Cary 50 UV-Visible spectrophotometer. The value of λmax of the BPB dye was determined by optical wide range scanning using the same equipment.

All dye removal experiments where performed using freshly prepared analytical grade dye solutions. Following the decolorization experiments, the absorbance was measured directly for solution aliquots and in some cases

further dilutions were made to account for high absorbance. All the experiments were performed under atmospheric pressure using polypropylene falcon tubes under shaking conditions.

2.3.1 Dye Removal Kinetics

The amount of Fe NPs used in this part was reduced to one tenth (0.0010g) of the amount used in the rest of dye removal experiment using Fe NPs, because the decolerization process was very fast to follow the kinetic changes at higher M/V ratios. But for Ni and Fe-Ni nanoparticles, the amount of adsorbent was 0.0100 g, because no change was observed in the dye concentration when 0.0010 g of adsorbents were used.

In order to study dye removal kinetics, the adsorbents (Fe, Ni, Fe-Ni NPs) were added separately to 25.0 mL of 100.0 mg/L BPB dye solutions. The mixtures were kept in contact periods in different falcon tubes. Subsequently, the dye solutions were separated from the adsorbents by filtration, and were analyzed using UV-Vis Spectrophotometry.

2.3.2 Effect of Initial Dye Concentration

The uptake capacity for each adsorbent was investigated by measuring the effect of initial dye concentration on the extent of dye removal. A fixed weight from Fe NPs and Fe-Ni NPs(1:1)S and (4:1)S adsorbent (0.0100 g) was mixed separately with 25.0 ml portions of BPB dye at initial concentrations of 20.0, 40.0, 60.0, 80.0 and 100.0 mg/L, and was kept in contact for 1 hour. The dye was then separated from the adsorbent by filtration.

In order to test the effect of temperature, the same experiments were repeated under the same conditions by adjusting the thermostat water bath at 323 K.

2.3.3 Effect of pH

The pH was adjusted to different values (4.0, 6.0, and 8.0) by using KHP or KH_2PO_4 buffers, in which the BPB powder was dissolved. The buffer solutions were prepared by dissolving the weights of KHP or KH_2PO_4 given in Table 2.2. Measured amounts of 0.1M HCl or NaOH was added, then deionized water was added to fill up to 1 liter volume to get the required pH.

Table 2.2 Amount of KHP or KH_2PO_4, HCl and NaOH used to prepare adjusted buffers at specific pH

pH	Mass of salt(g)	Volume of 0.1M HCl(mL)	Volume of 0.1M NaOH (mL)
pH=4	10.21 KHP	1	0
pH=6	6.81 KH_2PO_4	0	56
pH=8	6.81 KH_2PO_4	0	467

2.4 Characterization Techniques

2.4.1 Ultraviolet-Visible (UV-Vis) Spectrophotometry

The dye concentrations were measured using a Varian Cary 50 UV-Visible Spectrophotometer. The spectrophotometer operates on dual beam using a Czerny-Turner monochromator and working at 190–1100 nm wavelength range with approximately 1.5 nm fixed spectral bandwidth, the light source consists from full spectrum Xe pulse lamp, and has dual Si diode detectors.

The spectrophotometer was used to obtain calibration curves of Absorbance versus concentration for BPB (Fig. 2.1) dyes in the ranges of 1.0-10.0 mg L^{-1} respectively, at λmax equal to 590 nm.

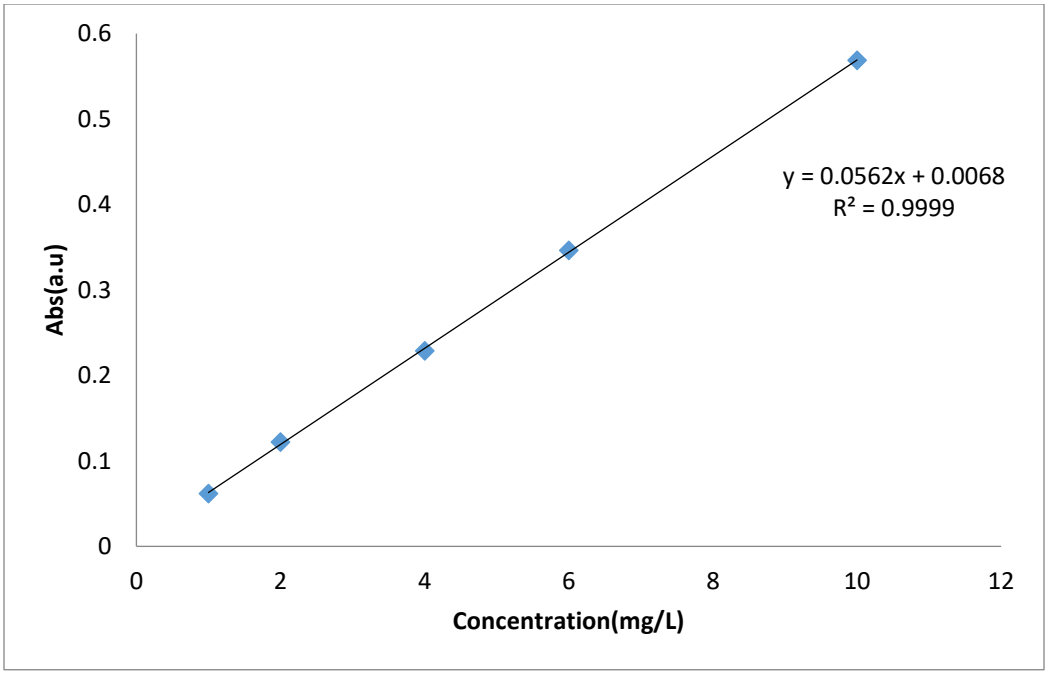

Figure 2.1 The calibration curve of bromophenol blue

2.4.2 Powder X-Ray Diffraction (XRD)

Powder XRD data were collected on a STOE Stadi P diffractometer with Cu Kα1 (λ = 1.54 Å) source at 40 kV/ 40 mA. The samples were scanned from 2θ of 5 to 80 degree located at Helmholtz Institute Ulm, Germany

2.4.3 Scanning Electron Microscopy (SEM)

The morphology of the nanoparticles were studied using Scanning Electron Microscopy (SEM) were recorded using a Hitachi, S-5200 field-emission scanning electron microscope, Hitachi, Tokyo, Japan. The accelerating voltage is 10 kV, and the images were taken with the secondary electron

detector, located at University of Ulm, electron microscopy department, Germany.

2.4.4 Transmission Electron Microscopy (TEM)

Transmission Electron Microscopy (TEM) images were recorded with a Jeol-1400 instrument, under an accelerating voltage of 120 kV, bright field signals. After preparation, the samples were placed on a copper grid and fixed on the device holder, and the parameters were adjusted to obtain clear images. The instrument is located at University of Ulm, electron microscopy department, Germany

During SEM and TEM analysis, the samples were dispersed in ethanol for few minutes using a sonicator, then one drop from the suspension was placed on a copper grid which then was fixed on a special holder and placed in the instrument.

2.4.5 X-Ray Photoelectron Spectroscopy (XPS)

X-ray photoelectron spectroscopy (XPS, Multiprobe, Omicron Nanotechnology) was performed in a multi-technique UHV instrument using a monochromatic Al Kα X-ray source (1486.7 eV, 270 W) and the chamber pressure was 5×10^{-10} mbar. The equipment is located at Physics department in Bielefeld University, Germany. The sample was dispersed in ethanol using

ultrasonic shaker path, then few drops of the suspension were placed on piece of silicon/silicon oxide substrate.

The analysis of the XP spectra was carried out using CasaXPS software, and a Shirley background subtraction procedure was employed.

2.4.6 Degradation Product Analysis:

In order to extract the dye degradation products, liquid-liquid extraction was performed with different types of organic solvents, such as diethyl ether, dichloromethane, chloroform, n-hexane and cyclohexane. Then the solution was checked extracted using UV-Vis Spectrophotometer if there is any peak at 317 nm.

Another method was used without extraction by loading the treated dye solution on thin layer chromatography (TLC) plate, and different mobile phases were used to separate the components based on polarities. Couples of organic solvents (polar and non-polar) with different volume ratios were used to change the polarity of the mobile phase. For example, diethyl ether with n-hexane used starting with diethyl ether to n-hexane (4:1) then gradually the percent of n-hexane to diethyl ether ratio was increased. other couples included dichloromethane -cyclohexane, chloroform-diethyl ether and dichloromethane- chloroform were used.

Chapter 3: RESULTS & DISCUSSION

3.1 Characterization the Synthesized Nanoparticles Materials

The characterization results of the prepared Fe NPs and bimetallic Fe-Ni NPs are provided and discussed in the following subsections.

3.1.1 Characterization of Fe NPs

The structure of Fe NPs was characterized using XRD to provide evidence about the presence of crystalline zero-valent iron in the sample. Fig. 3.1 shows the basic reflection of metallic iron (110 reflection) at 2θ= 44.9°. The reflections of iron oxides are very weak, indicating that nZVI is the major component of the Fe NPs material.[66]

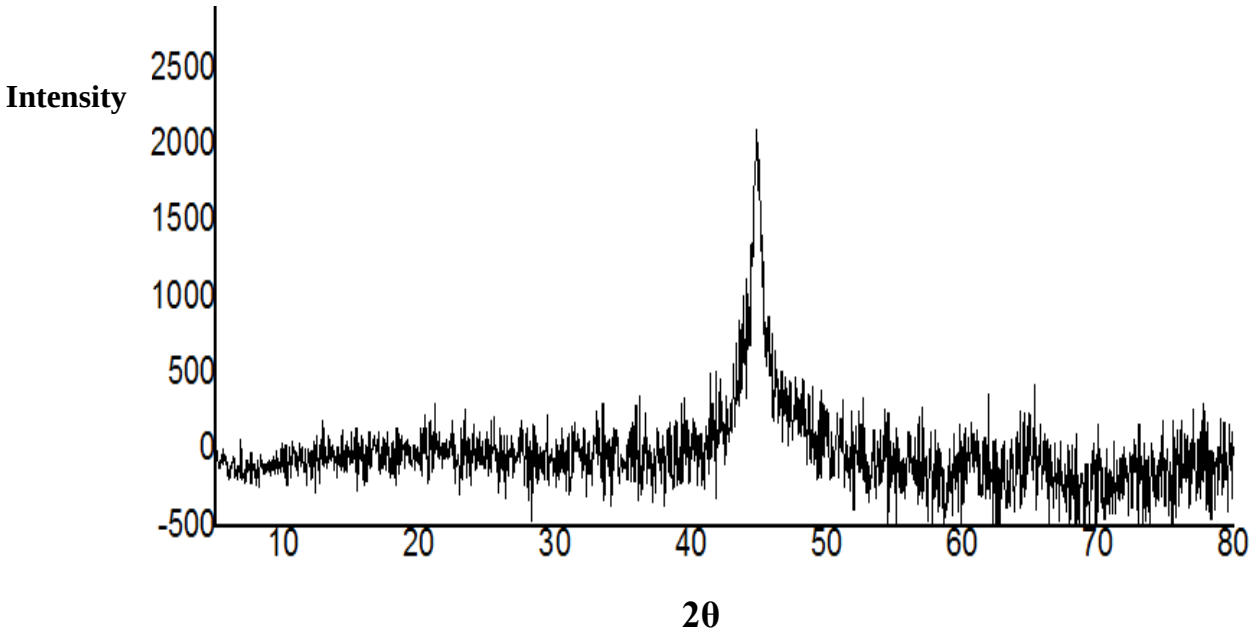

Figure 3.1 XRD pattern showing the basic reflections of Fe NPs

Typical SEM images of Fe NPs are shown in Fig. 3.2. The structure morphology of the iron sample matches with the results reported in earlier publications.[67,68,69] As shown in the SEM images, the diameter of individual Fe nanoparticles is in the range (40-80) nm, and it is aggregated into chain like structures; a typical behavior attributed to the magnetic attractive forces between the individual particles.

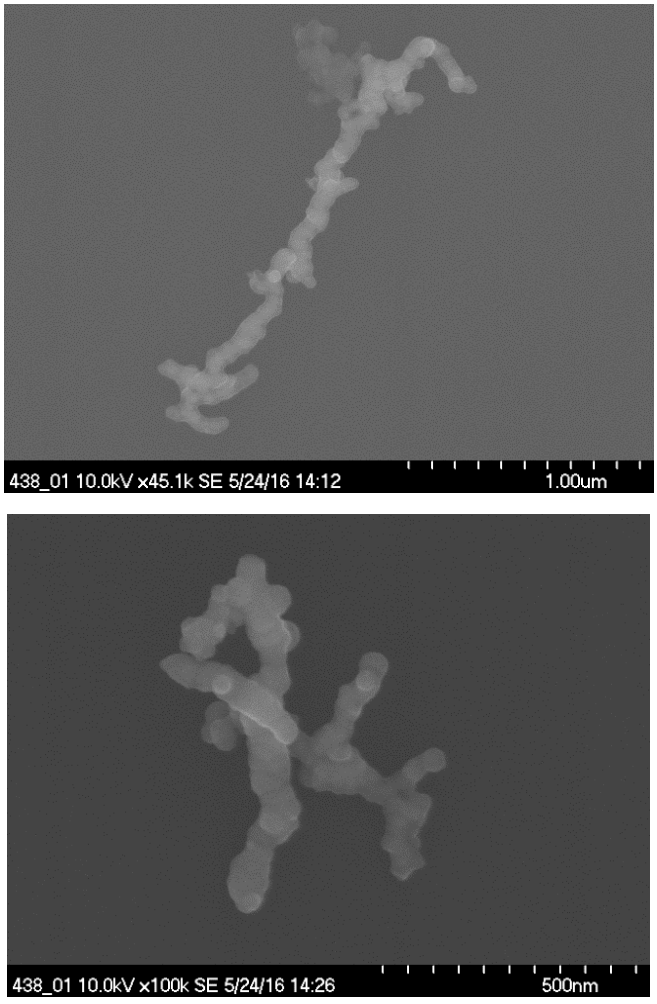

Figure 3.2 SEM images of Fe NPs at two different magnifications

Two typical TEM images of Fe NPs are given in Fig. 3.3. The dark color refers to the presence of iron and the lighter regions refer to the oxidized iron on the surface shells. It is well known that an Fe nanoparticle possesses a core-shell structure in which the core is composed of Fe in its (0) valence state, while the shell contains iron oxides and oxyhydroxides.[70]

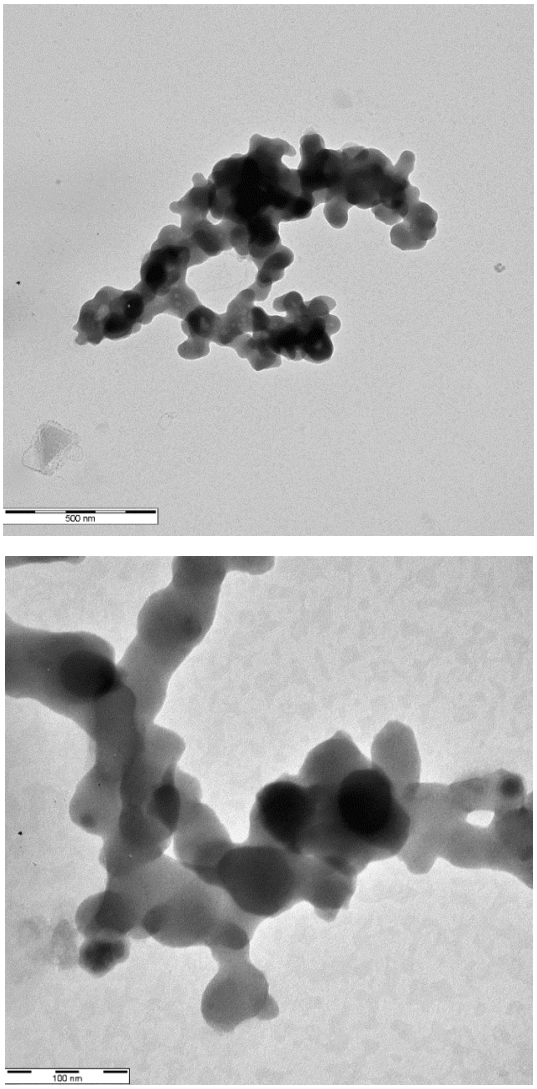

Figure 3.3 TEM images of Fe NPs at two different magnifications

The XPS analysis was performed at 13° emission angle. It was used to reveal the oxidation state(s) of iron and its surface composition. A wide XPS survey in addition to Fe 2p peak are shown in Figs. 3.4 and 3.5 respectively.

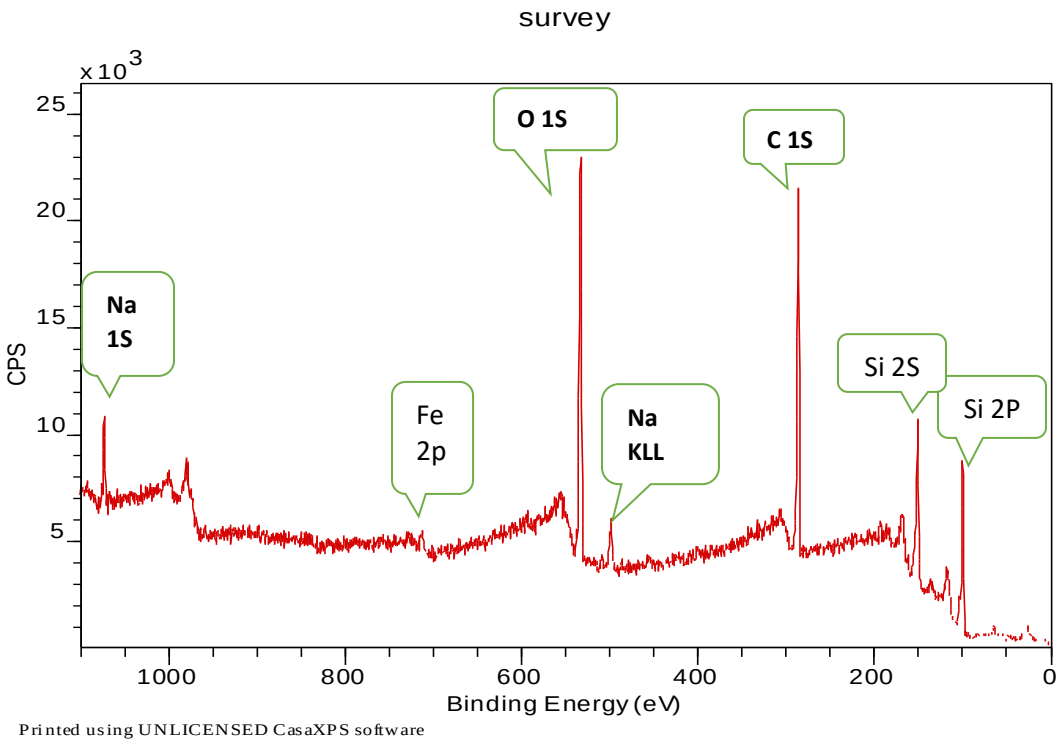

Figure 3.4 XPS spectrum for a sample of Fe NPs

The photoelectron peak at the binding energy of 285.5 eV corresponds to C 1s photoelectrons arising from adventitious sources. The O 1s feature appearing at 533 eV originates from O^{2-} in metal oxides.

The Fe 2p features at 727 eV and 713 eV, shown in Figure 3.5, are attributed to the binding energies of Fe $2p_{1/2}$ and $2p_{3/2,}$ respectively. The satellite peaks are observed around 720 and 730 eV. These features indicate that the shell in an Fe NP is

composed mainly of iron oxides and iron oxyhydroxides, as reported in earlier studies. The weak feature appearing at 707 eV arises from zero-valent iron (Fe^0). The results reflect the core-shell nature of nZVI.[71]

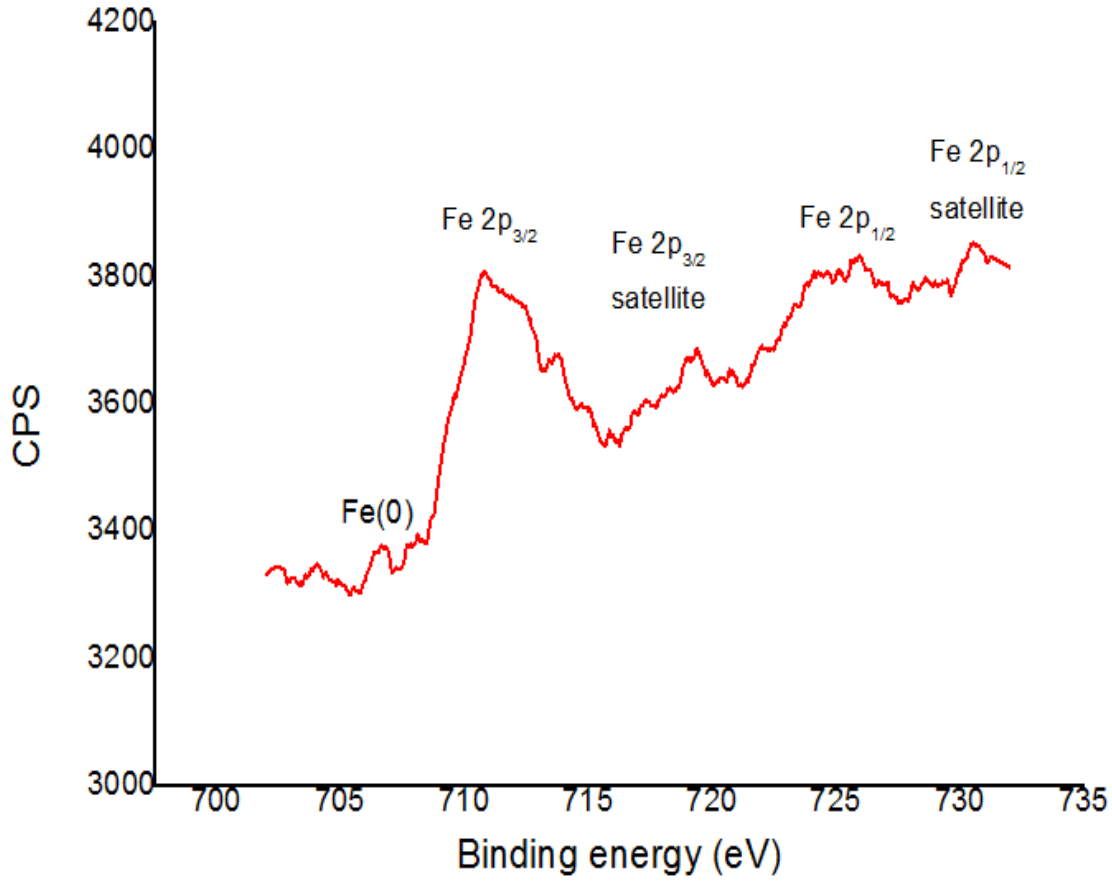

Figure 3.5 XPS features of Fe 2p in Fe NPs

3.1.2 Iron - Nickel Bimetallic Nanoparticles (Fe-Ni) NPs

The XRD pattern of a sample of Fe-Ni NPs is shown in Fig. 3.6. The broad peak centered at 2θ of 43-45 corresponds to the overlap between metallic Ni(111) major reflection (44.5°) and metallic Fe (110) major reflection (44.9°).[80,81]

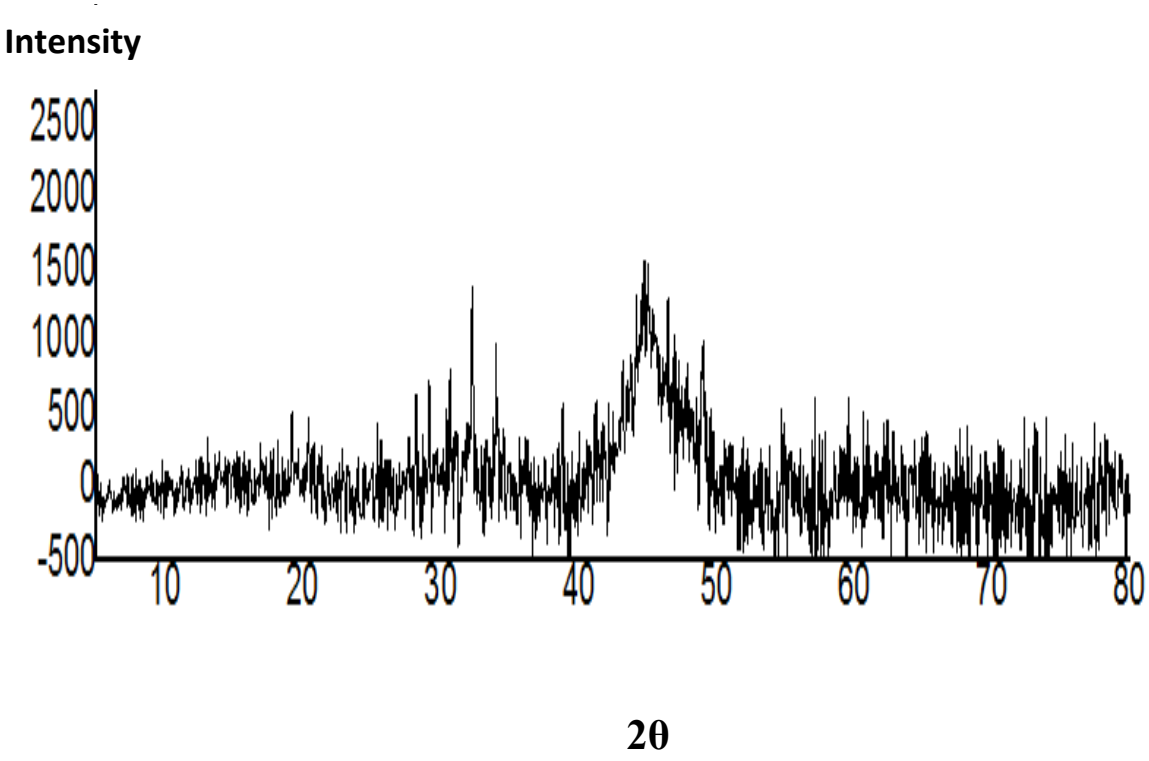

Figure 3.6 XRD pattern for Fe-Ni (4:1)S bimetallic nanoparticle

As given in literature, the XRD reflections of Ni occurs at 2θ= 27, 31.4, 33.6, 37.3 and 43.5° and the peak intensity is proportional to the percent of Ni in the sample. The peaks appear to be broad and the corresponding intensities are low indicating that the material is mostly amorphous.[72]

The SEM and TEM analysis of Fe-Ni bimetallic nanoparticles indicated aggregation due to the magnetic properties of Fe and Ni metals leading to the well known chain-like structure, as shown in Fig. 3.7. This is in line with earlier reports about this material.[46,40] The particle size appears to be smaller than that of Fe NPs, but the extent of aggregation seems to be more pronounced. In order to check the particle size, Helium ion microscope (HIM) analysis was performed. As can be seen in the image given in Fig. 3.8, the diameter of individual nanoparticles is approximatly 40-50 nm, which is roughly half of that observed for Fe NPs.

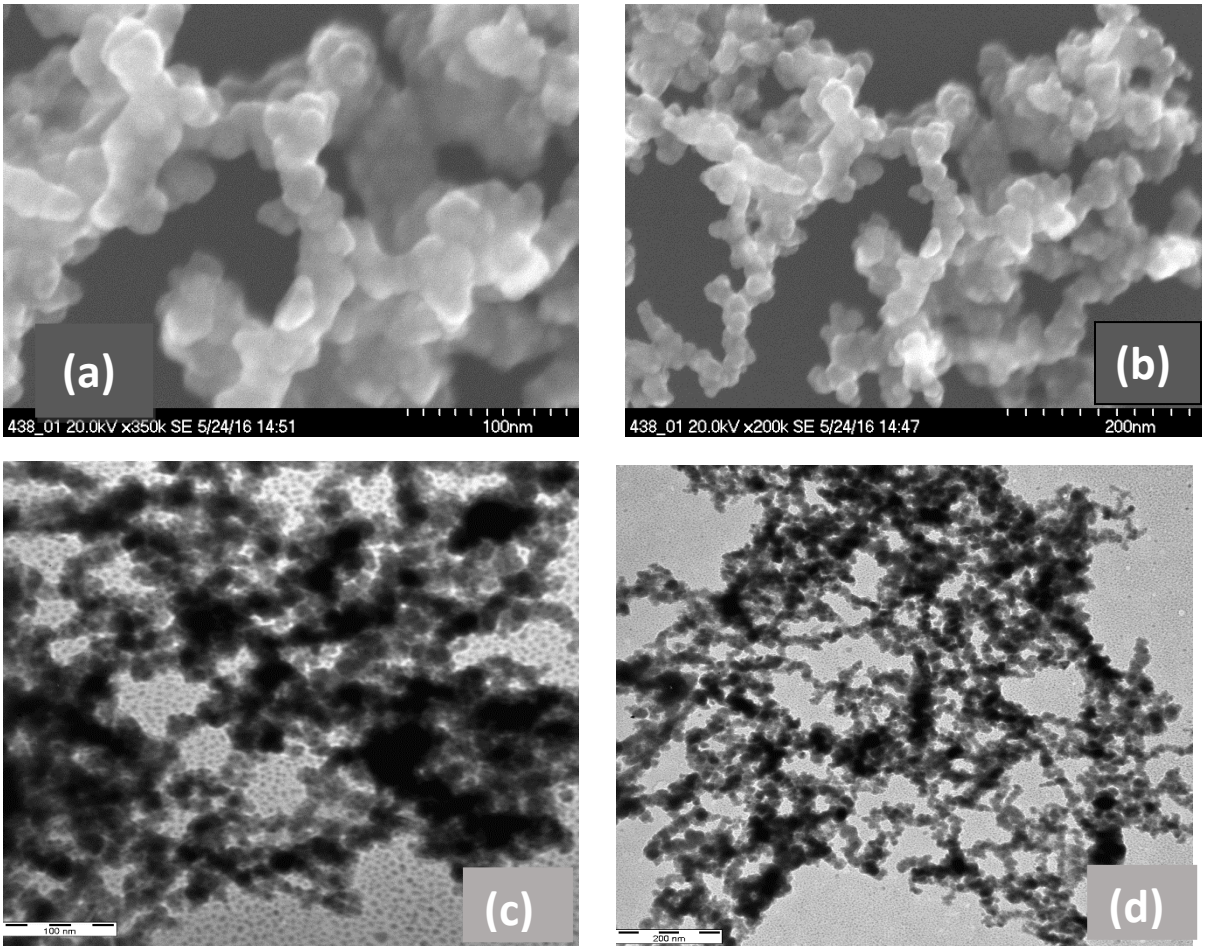

Figure 3.7 SEM (a,b) and TEM (c,d) images of Fe-Ni bimetallic nanoparticles

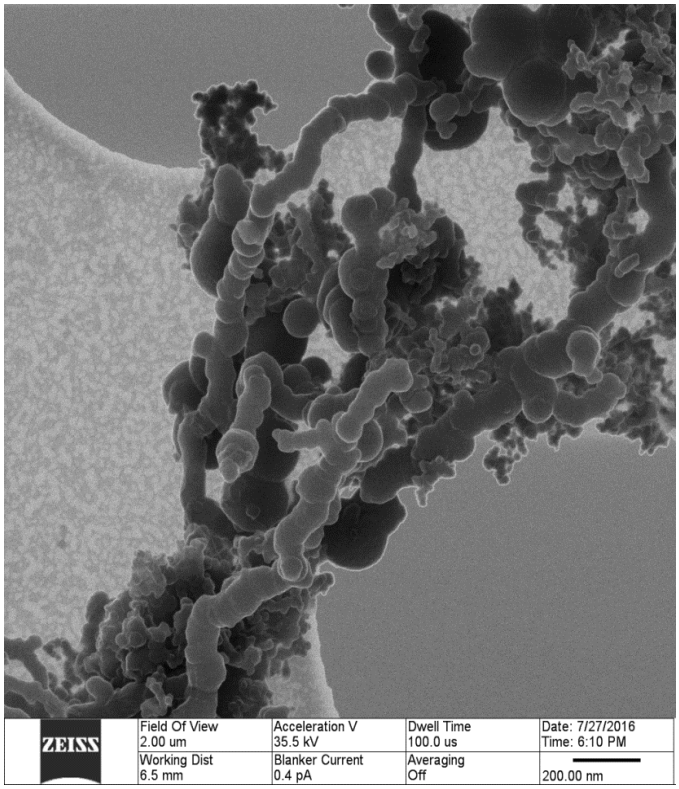

Figure 3.8 HIM analysis of Fe-Ni bimetallic nanoparticles

The wide scan XPS spectra of Fe-Ni (4:1)S sample is similar to that of Fe sample except that there are sulfur peak which arise from the source of iron used in the preparation of NPs ($FeSO_4$), in addition to the nickel peak, as shown in Fig. 3.9.

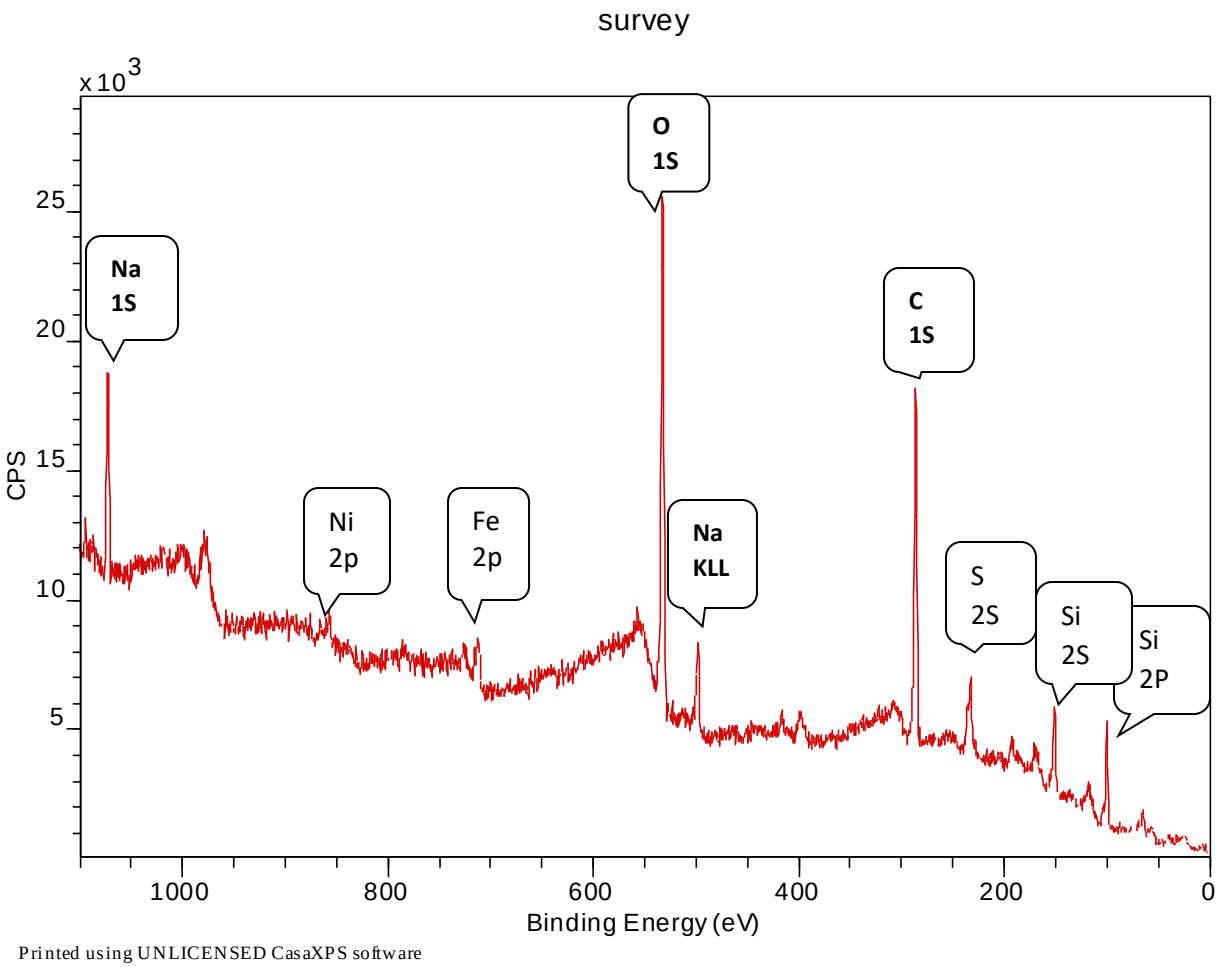

Figure 3.9 XPS analysis for (4:1)S Fe-Ni bimetallic NPs

For iron, the peak position is similar to that in pure Fe NPs, as shown in Fig 3.10. The nickel Ni2p has a spectral difference equal to 18 eV between Ni $2p_{3/2}$ and $Ni2p_{1/2}$, which are respectively observed at 857 eV and 875 eV. In addition, their satellite peak appeared at 863 and 883.5, respectively, as shown in Fig 3.11.[73]

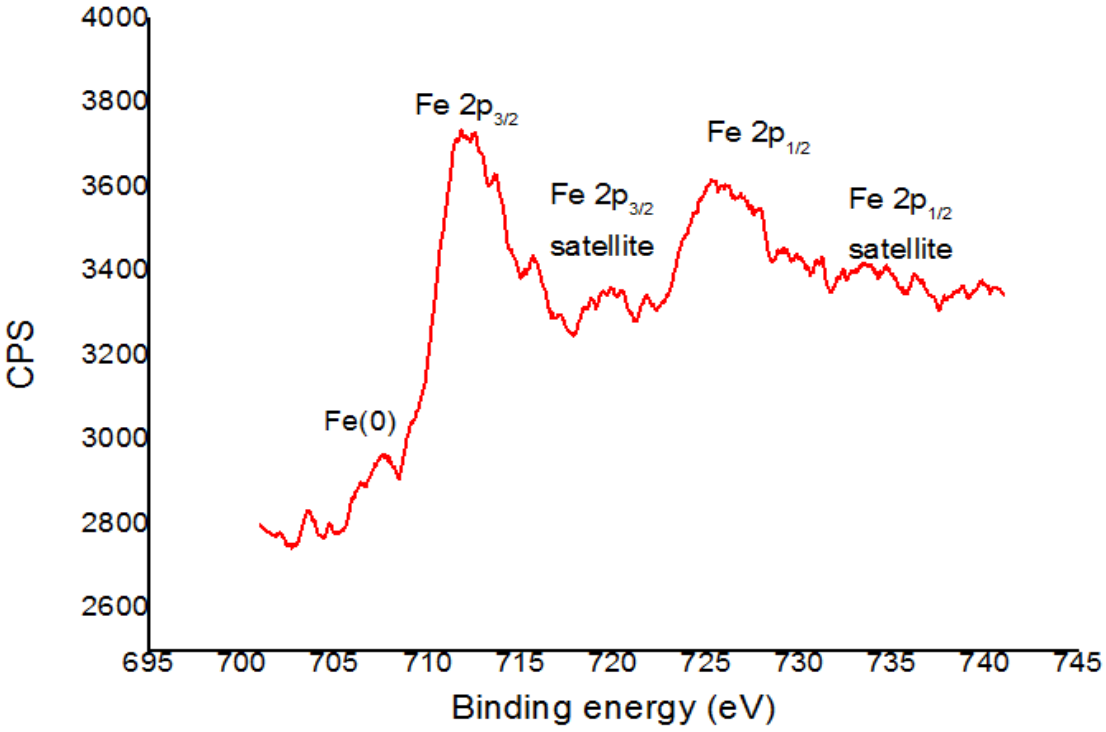

Figure 3.10 XPS features of Fe 2p in Fe-Ni NPs (4:1)S sample

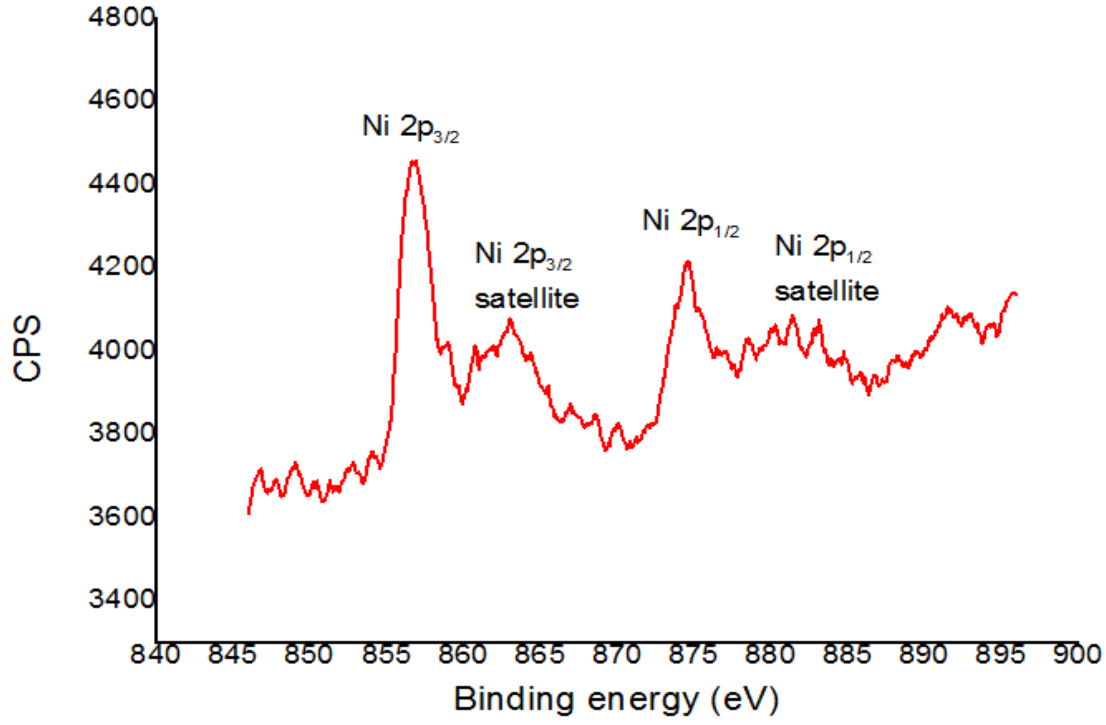

Figure 3.11 XPS features of Ni 2p in Fe-Ni NPs (4:1)S sample

While the XPS features in Fig. 3.10 corresponding to Fe 2p in Fe-Ni NPs show the presence of iron in its zero valent state (around 707 eV) no evidence is seen in Fig. 3.11 about the presence of zero valent nickel. On the overall, the extent of oxidation in Fe-Ni NPs is more pronounced compared with Fe NPs.

3.2 Effect of Sample Composition on the Removal Percentage of BPB

This study was performed as a preliminary test to elucidate the effect of iron and nickel content on the removal percentage of BPB.

The effect of Ni content (in Fe-Ni NPs) on the removal percentage of BPB is shown in Fig. 3.12. The nanoparticle material was synthesized from chloride salts of Fe and Ni, used as precursors.

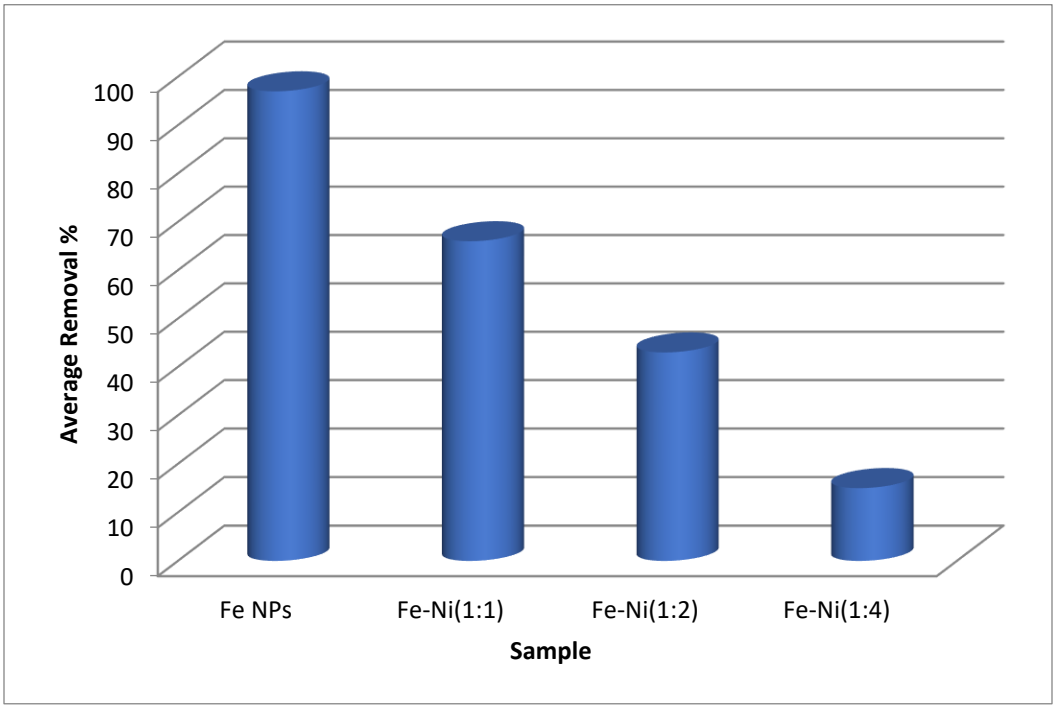

Figure 3.12 Effect of Ni content in Fe-Ni NPs on the removal % of BPB

As Fig. 3.12 shows, the removal percentage of BPB decreases as the nickel content is increased.

In addition, the iron salts used to prepare the iron-nickel bimetallic nanoparticles were changed. Two different iron to nickel (Fe: Ni) ratios were used which mare 1:1 and 4:1 ratios

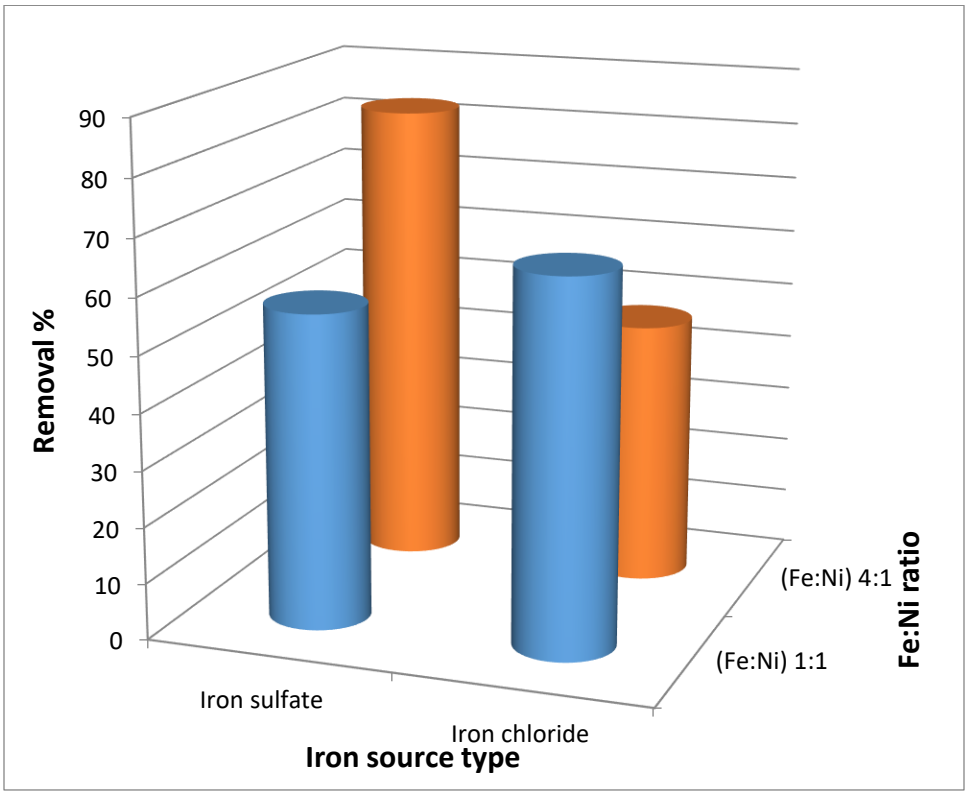

Figure 3.13 Effect of iron source on the removal %

From Fig. 3.13 it can be concluded that the highest dye removal is achieved when Fe-Ni ratio is 4:1, with ferrous sulfate used as precursor in the preparation of Fe-Ni NPs. Based on this, Fe-Ni (4:1)S was used in the further experiments of BPB removal. It was reported in literature that the type of iron source can affect the properties of iron oxide nanoparticles.[74]

3.3 Dye Removal Kinetics

Prior to performing the kinetic experiments, the removal of BPB dye was tested using three different doses of Fe NPs. The removal of the dye by Fe NPs was very fast and highly dependent on the amount of Fe NPs. Fig. 3.14 shows the percentage removal of BPB after 1 min. of contact with Fe NPs.

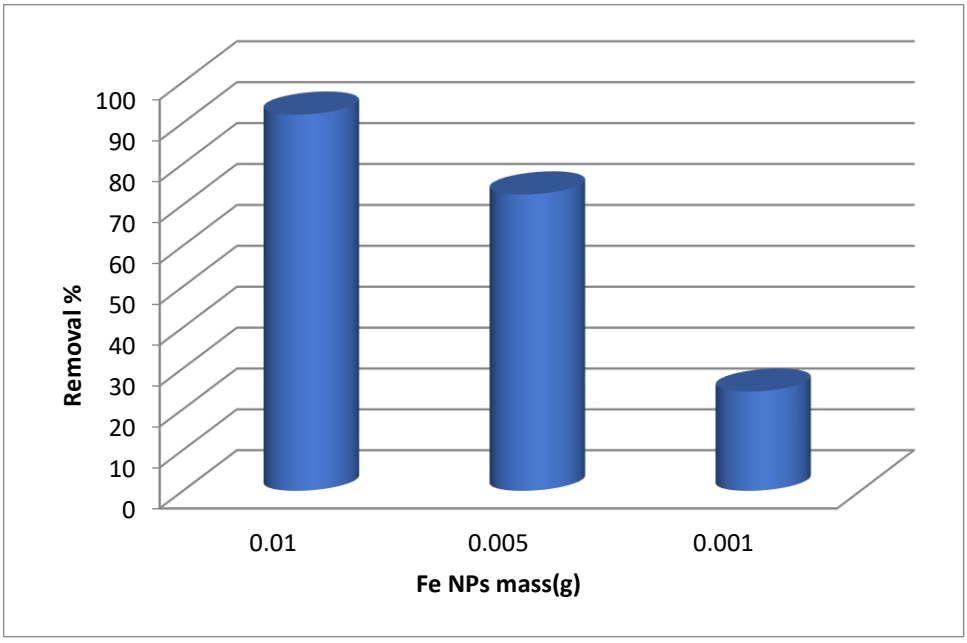

Figure 3.14 Effect of Fe NPs mass on the removal percentage of BPB

The kinetics experiments were performed for the samples which exhibited the highest removal potential; Fe NPs and Fe-Ni (4:1)S. For the sake of comparison, kinetic experiments were also performed using pure Ni NPs. Throughout the kinetics experiments, 0.0010 g portions of Fe NPs sample were used, because the reaction

was very fast at higher doses. However, in the case of Fe-Ni and Ni NPs, 0.0100 g was used due to low removal efficiency at 0.0010 g nanoparticle amount.

The kinetics data for the three types of nanoparticles are shown in Table 3.1, and these data are plotted in Fig 3.15.

The kinetic analysis showed that Fe and Fe-Ni NPs obey pseudo second order rate equation, but Ni NPs follow the pseudo first order rate equation.

Table 3.1 Variation of the BPB concentration (mg/L) with different contact times for Fe and Fe-Ni NPs.

	Fe	Fe-Ni
Time(min.)	[BPB](mg/L)	[BPB](mg/L)
0	100	100
1	81	69
2	67	59
5	66	46
10	50	38
15	44.2	32
30	47.6	34
60	47.5	16
240	47.2	22

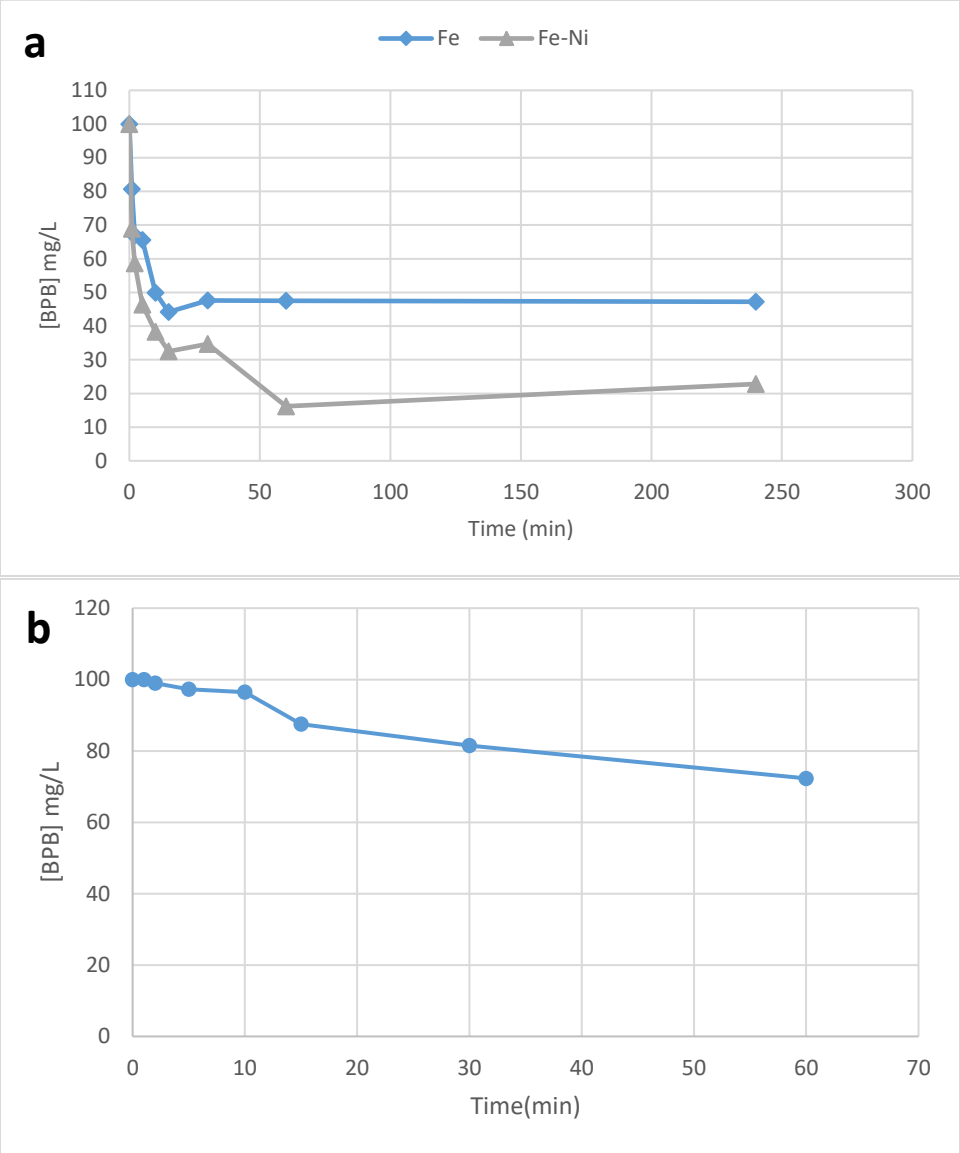

Figure 3.15 Variation of dye concentration with time: (a) for Fe and Fe-Ni NPs, (b) for Ni NPs

Although the removal mechanism may involve reductive degradation of BPB dye, adsorption of the dye molecules on the nanoparticles surface is essential as a preliminary step. The concentration of the dye on the solid surface can be linked to its liquid concentration through the mass balance equation given by: [75]

$$Q = (C_{\circ} - C)\frac{V}{m} \ldots\ldots\ldots\ldots\ldots\ldots\ldots (1)$$

Where, Q is the solute concentration on the solid (mg g^{-1}) at a given time,

C_0 is the initial solute concentration in solution (mg L^{-1}),

C is the solute concentration in solution at a given time (mg L^{-1}),

m is the mass of the sorbent (g),

V is the solution volume (L).

The relation between Q and t can be elucidated using various kinetic models employed in liquid-solid sorption systems. In this study, pseudo second order rate equations represented by Ho Equation[76] and Shahwan Equation[77] were used. As reported by their authors, these two equations were derived using two different approaches, and although the two equations look similar to each other, they differs in the interpretation of Q_e (or Q_m) and the method of determination of the rate constant, k, and its unit.

The nonlinear form of Ho equation is given as:

$$Q = \frac{K.t.Qe^2}{1+K.Qe.t} \ldots\ldots\ldots\ldots\ldots\ldots\ldots (2)$$

It can be linearized to;

$$\frac{t}{Q} = \frac{1}{KQe^2} + \frac{1}{Qe}\,t \quad \text{……..... (3)}$$

Where Q_e is the experimental value of Q at the equilibrium, and k is the rate constant.

On the other hand, the nonlinear and linearized forms of Shahwan equation are given as:

$$Q = \frac{Q_m C_\circ K t}{C_\circ K t + 1} \quad \text{…… (4)}$$

$$\frac{t}{Q} = \frac{1}{Q_m C_\circ K} + \frac{1}{Q_m}\,t \quad \text{……..... (5)}$$

Where, Q_m is the maximum amount of solute that would be sorbed if the sorption reaction goes to completion (equals to *V/ m multiplied by* C_0), and k is the rate constant.

The linear fits of the kinetic data of Fe and Fe-Ni cases obtained using the linearized equations of Ho (Eq. 3) and Shahwan (Eq. 5) models are shown in Fig. 3.16.

The data used in the plots correspond to the pre-equilibrium stage of the experiments. Fundamentally, the kinetic analysis is applicable to the variation of concentration with time, which occurs during the initial stage of the experiment.[77]

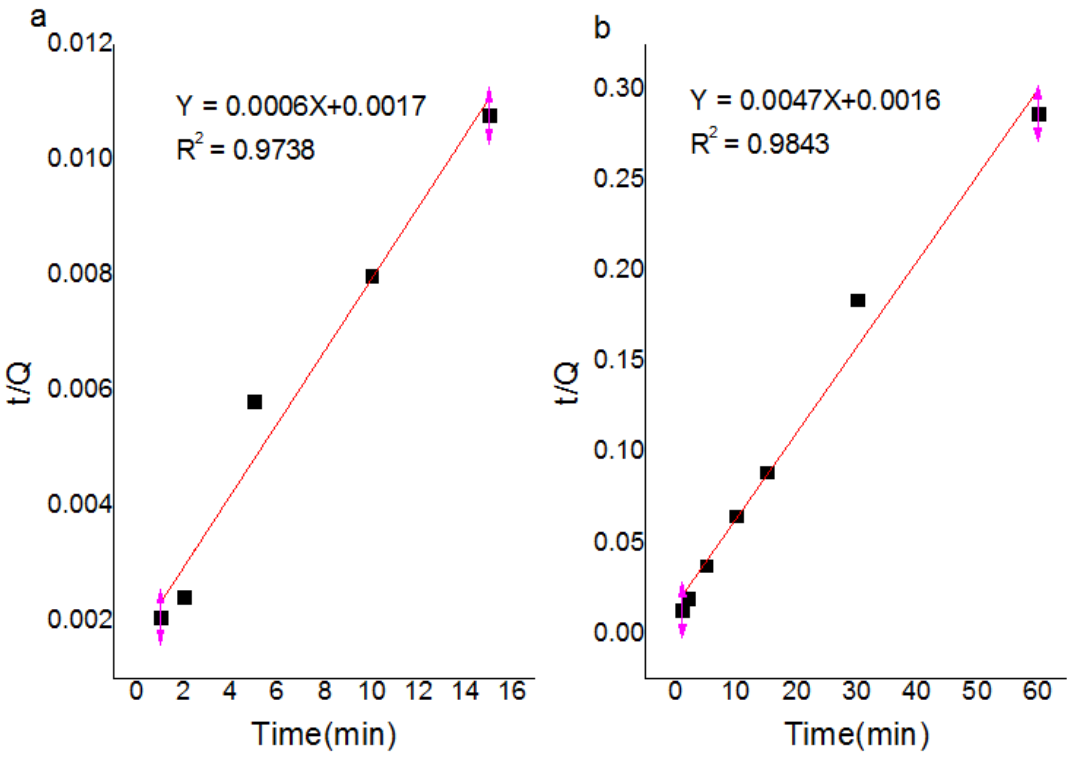

Figure 3.16 Pseudo second order linear fits for the removal of BPB by: (a) Fe NPs (b) Fe-Ni NPs.

Linear regression is the most commonly used method to obtain the parameters involved in the kinetic equations and also in predicting the best fitting kinetic expression.

The calculated kinetic rate constants, the corresponding coefficients of determinations (r^2), theoretical Q values, and the half-life ($t_{1/2}$) are given in

Table 3.2.

Table 3.2 Kinetic constants for BPB onto Fe and Fe-Ni NPs by linear regression analysis method

Nanoparticles	Parameter	Ho Equation	Shahwan Equation
Fe	Slope	0.00060	0.00060
	Intercept	0.0017	0.0017
	Coefficient of determination, r^2	0.9738	0.9738
	Rate constant, k	0.000212 $g.mg^{-1}.min^{-1}$	0.00353 $L.mg^{-1}.min^{-1}$
	Experimental Qe (or Qm), mg/g	1320	1320
	Model value of Qe (or Qm),mg/g	1667	1667
	Experimental $t_{1/2}$, min.	10	10
	Theoretical $t_{1/2}$, min.	47.2	2.8
Fe-Ni	Slope	0.0047	0.0047
	Intercept	0.0016	0.0016
	Coefficient of determination, r^2	0.9843	0.9843
	Rate constant, k	0.001381	0.00294
	Experimental Qe (or Qm), mg/g	208	208
	Model value of Qe (or Qm)	213	213
	Experimental $t_{1/2}$, min.	4	4
	Theoretical $t_{1/2}$, min.	7.2	3.4

Since the linear plots of Ho and Shahwan equations are the same, the slope and the intercept are identical but the calculated parameter such as k and $t_{1/2}$ are different.

As Table 3.2 shows, Shahwan equation provides closer value of $t_{1/2}$ to the experimental one. The results indicate that the rate constant of BPB removal by Fe NPs is higher than the one for Fe-Ni, thus verifying a faster removal process by Fe NPs.

The value of k calculated using Shahwan equation was always higher than k value calculated using Ho equation. To check which of the two equations provide closer correlation with the experimental results, the calculated k and Q values were substituted in the nonlinear equations (2&4) and the calculated Q (or the model prediction) values were plotted together with the experimental values.

As shown in Fig. 3.17, for Fe NPs kinetic experiment, the nonlinear fit using Shahwan equation is better fit to the experimental data than Ho equation.

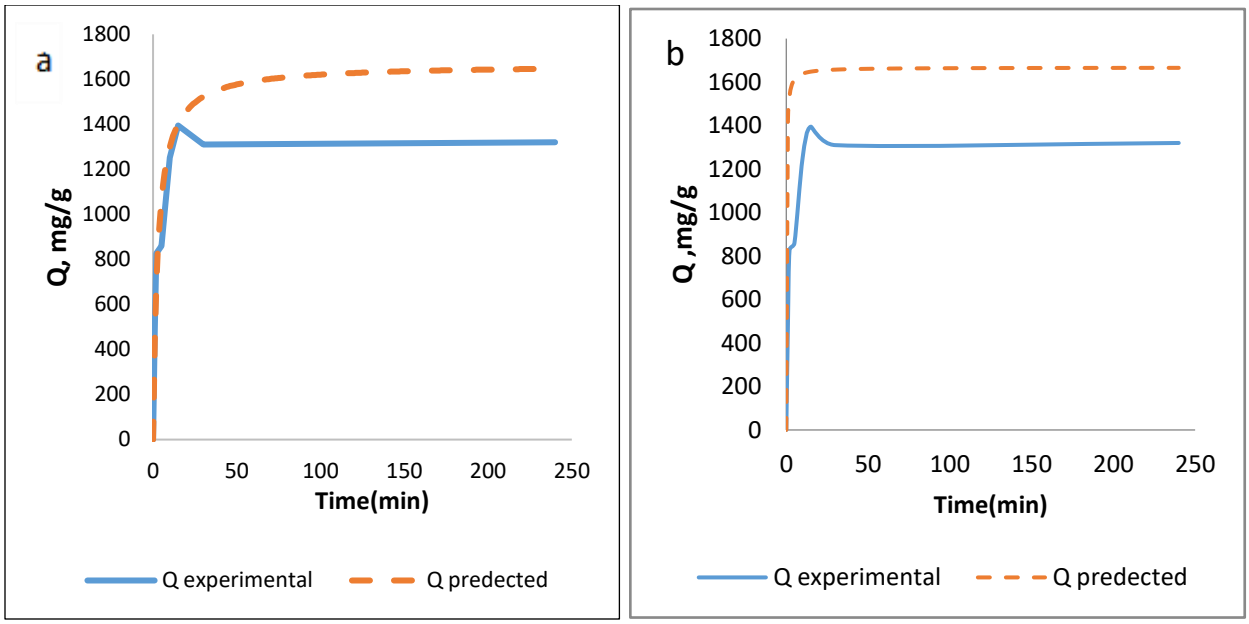

Figure 3.17 Nonlinear fits of the kinetic data of BPB removal by Fe NPs; (a) using Shahwan equation (b) using Ho equation.

On the other hand, for Fe-Ni NPs, the two models showed similar correlation, as shown in Fig 3.18.

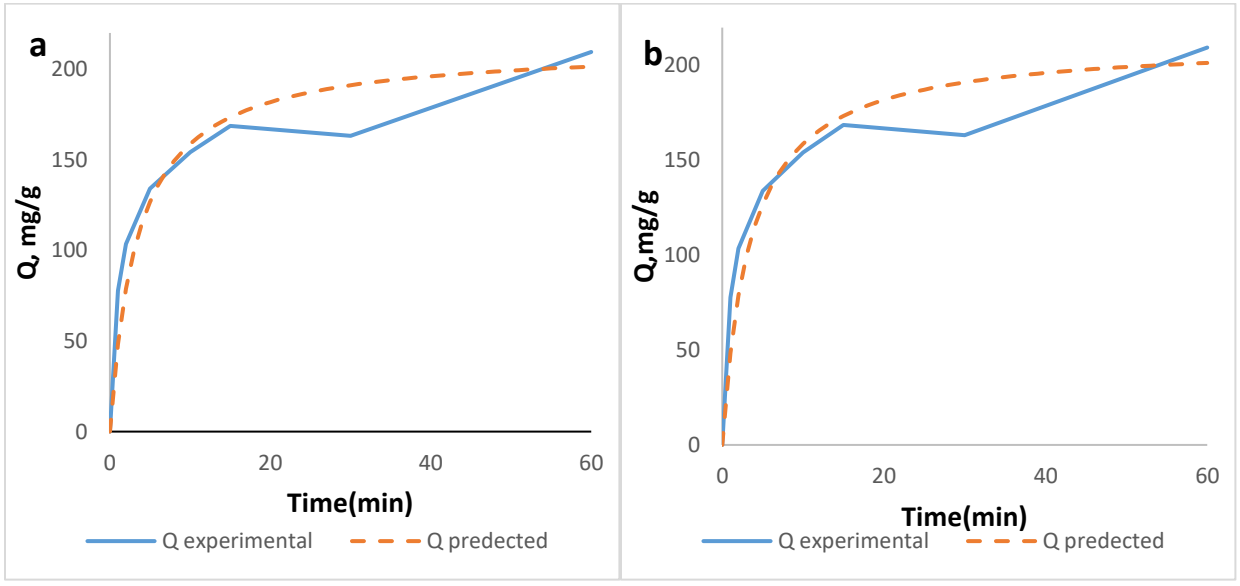

Figure 3.18 Nonlinear fits of the kinetic data of BPB removal by Fe-Ni NPs; (a) using Shahwan equation (b) using Ho equation.

As a further test of the correlation, the Chi test was performed. For this purpose the following equation was used:

$$\chi^2 = \sum_{1}^{n} \frac{\left(Q_{exp} - Q_{model} \right)^2}{Q_{model}}$$

The Chi test results express the compatibility between the experimental and predicted value of Q. The smaller the value of χ^2 means that the difference between experimental and predicted values is smaller. Table 3.3 shows the values of χ^2 for two models of Shahwan and Ho using Fe and Fe-Ni NPs. For dye removal kinetics by Fe NPs, the Chi test results indicate that the Q values predicted by Shahwan equation are closer to the experimental value more than Q values predicted by Ho equation. On the other hand, the Chi test for the dye removal kinetics by Fe-Ni NPs exhibit similar values.

Table 3.3 Values of Q obtained from experiment, values of Q_m predicted by Shahwan model, values of Q_e predicted by Ho model, and the Chi-test values for the two sorption systems.

Time	Q (mg/g)	Q_m (mg/g)	Chi test (Shahwan model)	Q_e (mg/g)	Chi test(Ho model)
Fe NPs					
1	482.5	434.8	5.2	1424.5	622.9
2	827.5	689.6	27.6	1536.1	326.9
5	860	1063.8	39	1611.9	350.7
10	1252.5	1298.7	1.6	1638.8	91.1
15	1395	1401.9	0.034	1648	38.8
30	1310	1522.9	29.8	1657.3	72.8
60	1312.5	1591.5	48.9	1661.9	73.5
240	1320	1647.2	65	1665.5	71.7
		χ^2	217.2	χ^2	1648.4
Fe-Ni NPs					
1	77.75	48.3	17.9	48.3	17.9
2	103.5	78.7	7.8	78.8	7.8
5	134	126.6	0.4	126.6	0.4
10	154.25	158.8	0.13	158.8	0.13
15	168.75	173.4	0.13	173.4	0.13
30	163.25	191.1	4.1	191.1	4.1
60	209.5	201.4	0.33	201.4	0.33
240	212.5	201.4	0.62	201.4	0.61
		χ^2	31.38	χ^2	31.35

On the other hand, unlike the kinetic data of Fe and Fe-Ni NPs, the data of BPB removal by Ni NPs correlated better with the pseudo first order rate equation (Lagergren Equation), given as;[75]

$$\ln(Q_e - Q) = lnQ_e - kt \quad \ldots\ldots\ldots\ldots (7)$$

In addition, a modified form of Lagergren equation, suggested by Shahwan, was also tried. In this form, Q_e is replaced by Q_m:[74]

$$\ln(\ Q_{max} - Q\ ) = \ lnQ_{max} - kt \quad \ldots\ldots (8)$$

Q_{max} can be calculated by:

$$Q_{max} = (V/m\ ) * C_0$$

The kinetic data of Ni NPs case were plotted using the two equations as shown in Fig 3.19. Both equations (original and modified Lagergren equations yield close results as seen in Table 3.4.

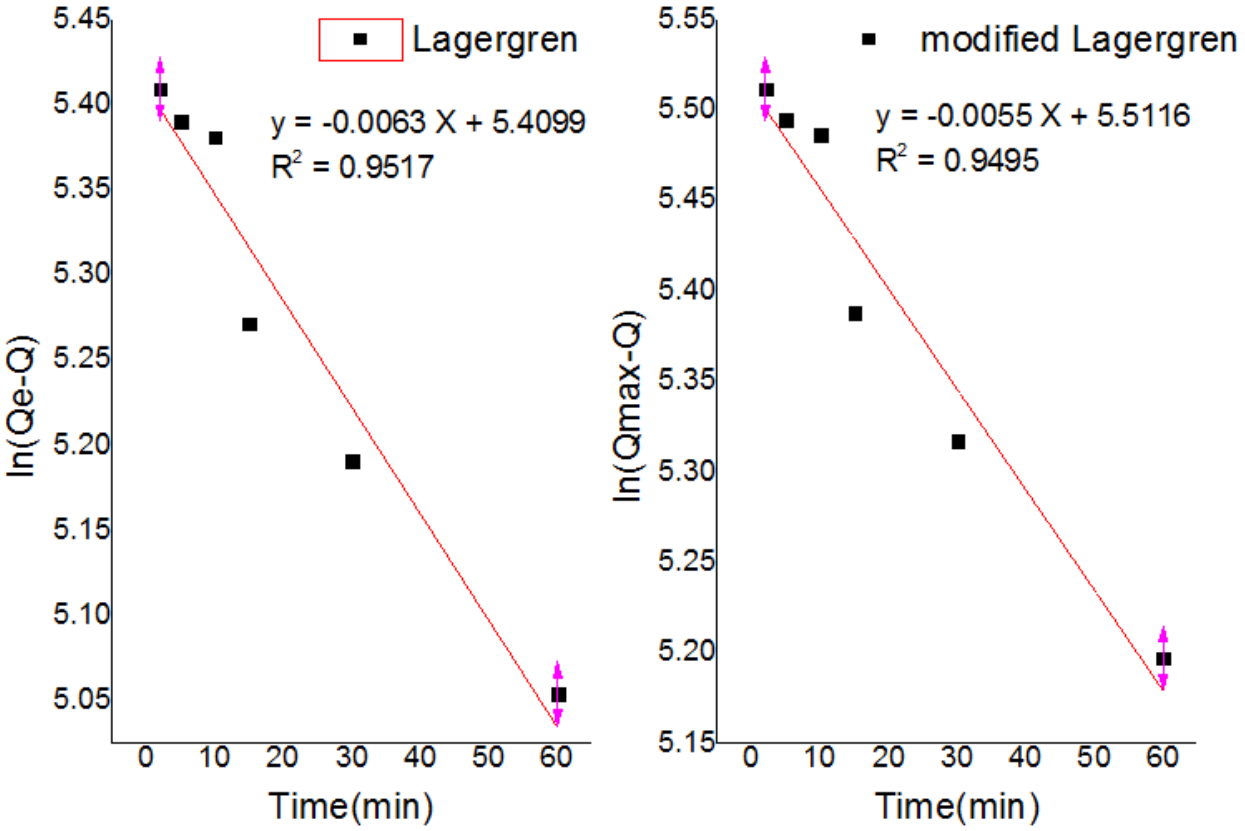

Figure 3.19 Pseudo first order linear fit for Ni NPs using original Lagergren equation and modified Lagergren equation

Table 3.4 Kinetic constants for BPB removal by Ni NPs.

	Modified Lagergren Equation	**Original Lagergren Equation**
Slope	-0.0055	-0.0063
Intercept	5.5116	5.4099
Coefficient of determination, r^2	0.9495	0.9517
Rate constant, k (min^{-1})	0.0055	0.0063
Experimental Q_e (or Q_m) (mg/g)	250	225.9
Model value of Q_e (or Q_m) (mg/g)	247.5	223.6
Experimental $t_{1/2}$, min.	120	120
Theoretical $t_{1/2}$, min.	126	110

The non- linear fit of original and modified Lagergren equation of nickel kinetic data exhibit similar correlation between the experimental and calculated data as shown in Fig 3.20

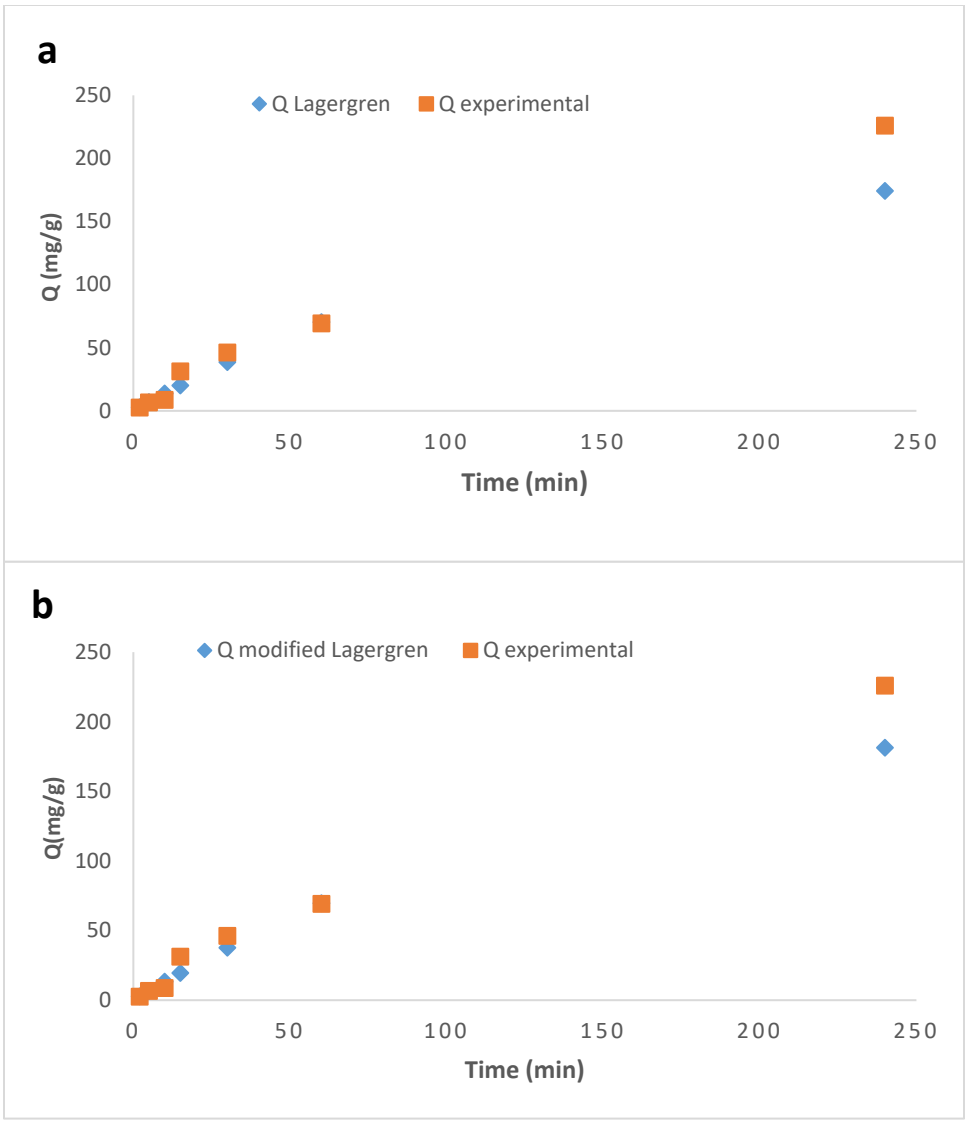

Figure 3.20 Nonlinear fits of the kinetic data of BPB removal by Ni NPs; (a) using Lagergren equation (b) using modified Lagergren equation.

Table 3.5 summarizes the kinetic parameters of the three sorption systems. The dye removal using Fe and Fe-Ni NPs follows the pseudo second order fit, but the dye removal with Ni NPs follows pseudo first order.

Table 3.5 values of k and Q_m for the three sorption systems

NPs	r^2	k	Q_m(mg/g)
Fe	0.9738	0.0035	2500
Fe-Ni	0.9843	0.0029	250
Ni	0.9838	0.0094	250

It can be concluded that the effectiveness of the Fe-Ni NPs in dye removal is less than of Fe NPs, and this is further confirmed by the lower efficiency of Ni NPs. The Ni NPs seems to take longer time to remove BPB compared with Fe NPs (maximum 10 min) for complete dye removal using the same weight of adsorbents (0.0100 g).

3.4 Effect of Initial Dye Concentration

The effect of initial BPB concentration on the extent of dye removal was investigated using Fe NPs and two types of Fe-Ni NPs prepared at different Fe:Ni ratios, as explained in the experimental part. The Fe-Ni NPs are marked as (4:1)S and (1:1)S. The studied initial dye concentrations were 20.0, 40.0, 60.0, 80.0 and 100.0 mg L^{-1}. The time of contact was kept at 1 hour, and the experiments were conducted at 298 K. The obtained results are provided in Table 3.6.

The results indicate that Fe NPs are superior in BPB removal at all studied concentrations. Among the two Fe-Ni NPs samples, the (4:1)S sample showed highest BPB removal.

In order to elucidate the partitioning of BPB among liquid and solid phases, isotherm fits were performed. For this purpose, a new approach was used, which is based on the linear isotherm combined with the mass balance equation. Based on this, a relation between the sorbed BPB amount (Q) and its initial concentration (C_0) was formulated. This enabled calculation of "apparent" equilibrium constants which are valid over the studied concentration range.

The linear isotherm is given by the relation:

$$Q=KC \cdots\cdots\cdots\cdots \quad (8)$$

K is a proportionality constant, which stands for a distribution ratio of the solute between the solid and liquid phases. The linear isotherm stands as a special case of Freundlich isotherm (KC^n), and relates the equilibrium liquid concentration of a solute to its concentration on the solid over a particular range of concentration.

The mass balance equation for a single stage batch process is given as:

$$Q = (C_\circ - C)\frac{V}{m} \quad \text{……. (9)}$$

Substituting for C from the mass balance equation, the linear isotherm becomes:

$$Q = K\left(C_\circ - \frac{Q.m}{V}\right) \quad \text{····· (10)}$$

Rearranging;

$$Q = \frac{K}{1+\frac{K.m}{V}}\, C_\circ \quad \text{····· (11)}$$

Since K, m, and V are all constants, the equation above can be expressed as:

$$Q = K` C_\circ \quad \text{····· (12)}$$

Where $K` = \frac{K}{1+\frac{K.m}{V}}$

Thus K` can be obtained from the slope of Q vs C_0 plots, and can subsequently be used to calculate K using the equation:

$$K = \frac{K'}{1-\frac{K'.m}{V}} \quad \ldots\ldots\ldots\ldots\ldots\ldots \quad (13)$$

The K values were then used to calculate standard Gibbs energy change (ΔG°) values using the well-known thermodynamic relation:

$$\Delta G^{\circ} = -RTlnK \quad \ldots\ldots\ldots\ldots\ldots \quad (14)$$

Table 3.6 The calculated Q values of BPB on three different NPs types at various BPB initial concentrations.

	Q (mg/g)		
	Fe NPs	Fe-Ni NPs	
C_0 (mg/L)		(4:1)S	(1:1)S
20	47	39	36
40	96	82	71
60	141	116	118
80	194	159	125
100	243	218	140

The data in Table 3.6 were fitted separately as shown in (Fig. 3.21) and the slope of each figure was used to calculate K` and K values, which were then used to obtain ΔG° values, as provided in Table 3.7.

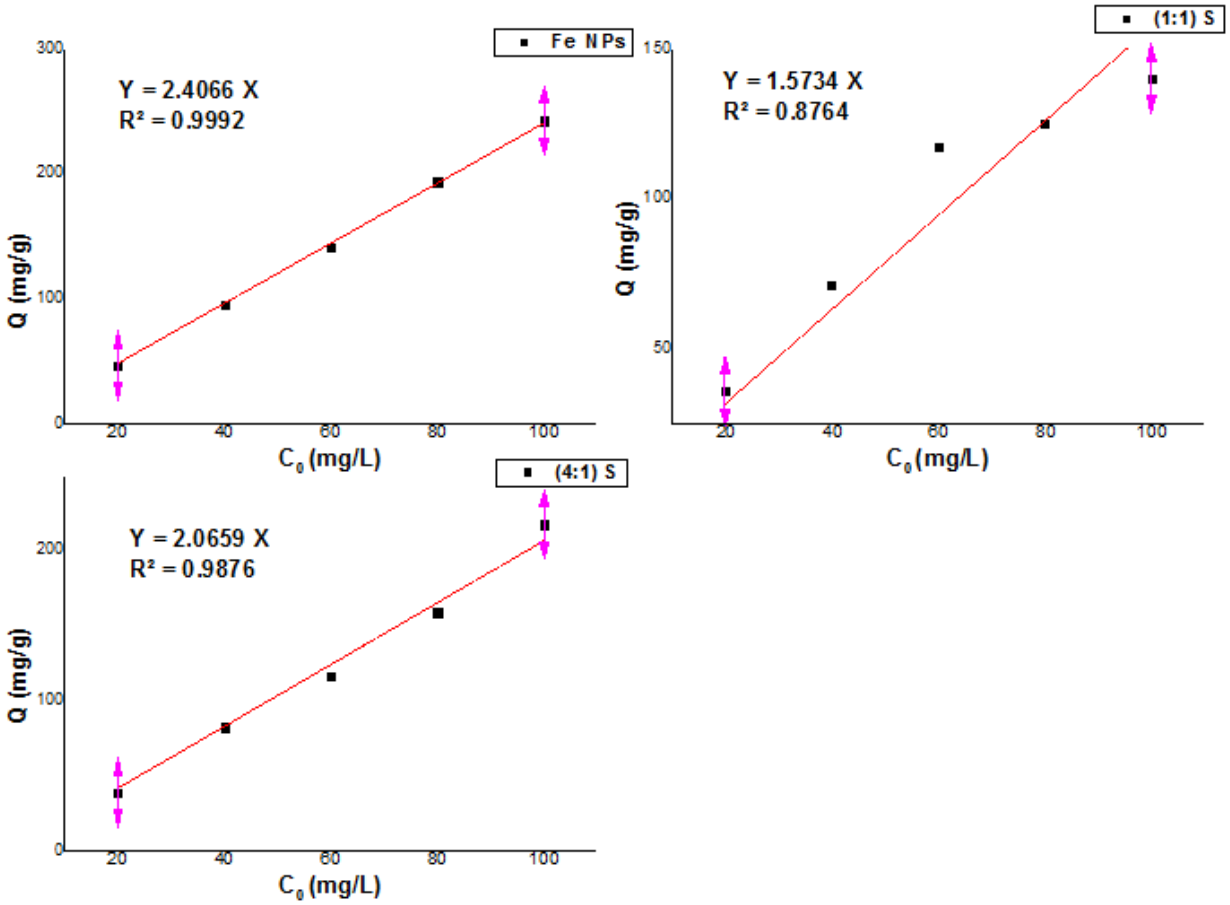

Figure 3.21 Variation of Q with C_0 for BPB using three different NPs types: Fe NPs, Fe-Ni NPs (1:1) S and Fe-Ni NPs (4:1) S.

Table 3.7 Values of coefficient of determination (R^2), K`, K, and ΔG˚ obtained for sorption of BPB on three different NPs types at 298 K.

	sample	slope	R^2	K'(ml/g)	K (ml/g)	ΔG˚ (kJ/mol)
Fe NPs	Fe	2.4066	0.9992	2406	64416	-27.4
Fe-Ni NPs	(1:1) S	1.5734	0.8764	1573	4245	-20.7
	(4:1) S	2.066	0.9876	2066	11901	-23.2

The table indicates that Fe NPs are more effective than both types of Fe-Ni NPs, as reflected by the higher K values. In all cases, the sorption reactions favors the products over the reactants, as indicated by the negative ΔG˚ values, which is seen to increase as iron content in the nanoparticles increases.

3.5 Effect of Temperature:

The effect of increasing the temperature from 25.0 ℃ to 50.0 ℃ on the extent of dye removal using Fe and Fe-Ni nanoparticles was studied at the initial dye concentrations of 20, 40, 60, 80.0 and 100.0 mg/L. The mixture components were kept in contact for 1 hour.

The standard enthalpy change was calculated using Van't Hoff equation:

$$\ln \frac{K_2}{K_1} = -\frac{\Delta H^0}{R}\left(\frac{1}{T_2} - \frac{1}{T_1}\right) \ldots\ldots\ldots (15)$$

Where the "apparent" equilibrium constant (K) was calculated using the same approach used in the part of initial day concentration effect.

The value of standard entropy change, ΔS°, was calculated using the following equation:

$$\Delta S^\circ = \frac{\Delta H^\circ - \Delta G^\circ}{T} \ldots\ldots\ldots\ldots (16)$$

The obtained results are shown in Table 3.8.

Table 3.8 Values of Q obtained for sorption of BPB on Fe and Fe-Ni at 298 K and 323 K using different initial dye concentrations.

	Q (mg/g)			
	298 K		323 K	
C_0(mg/L)	Fe	Fe-Ni	Fe	Fe-Ni
20	47	39	45	23
40	96	82	91	48
60	141	116	138	73
80	194	159	181	100
100	243	218	219	119

The data displayed in (Table 3.8) showed three main trends:

1. Q increases as the initial concentration increases,
2. Q values are higher for BPB removal by Fe NPs,
3. For both type of NPs, Q decreased with increasing temperature.

These experimental data was fitted using equation 12, as shown in Fig. 3.22, and the slope of each figure was used to calculate K` and K values. The obtained K values were calculated using equation 13. The K values were then used to obtain ΔG° values, ΔH° and ΔS° (using equations 14, 15 and 16), as provided in Table 3.9.

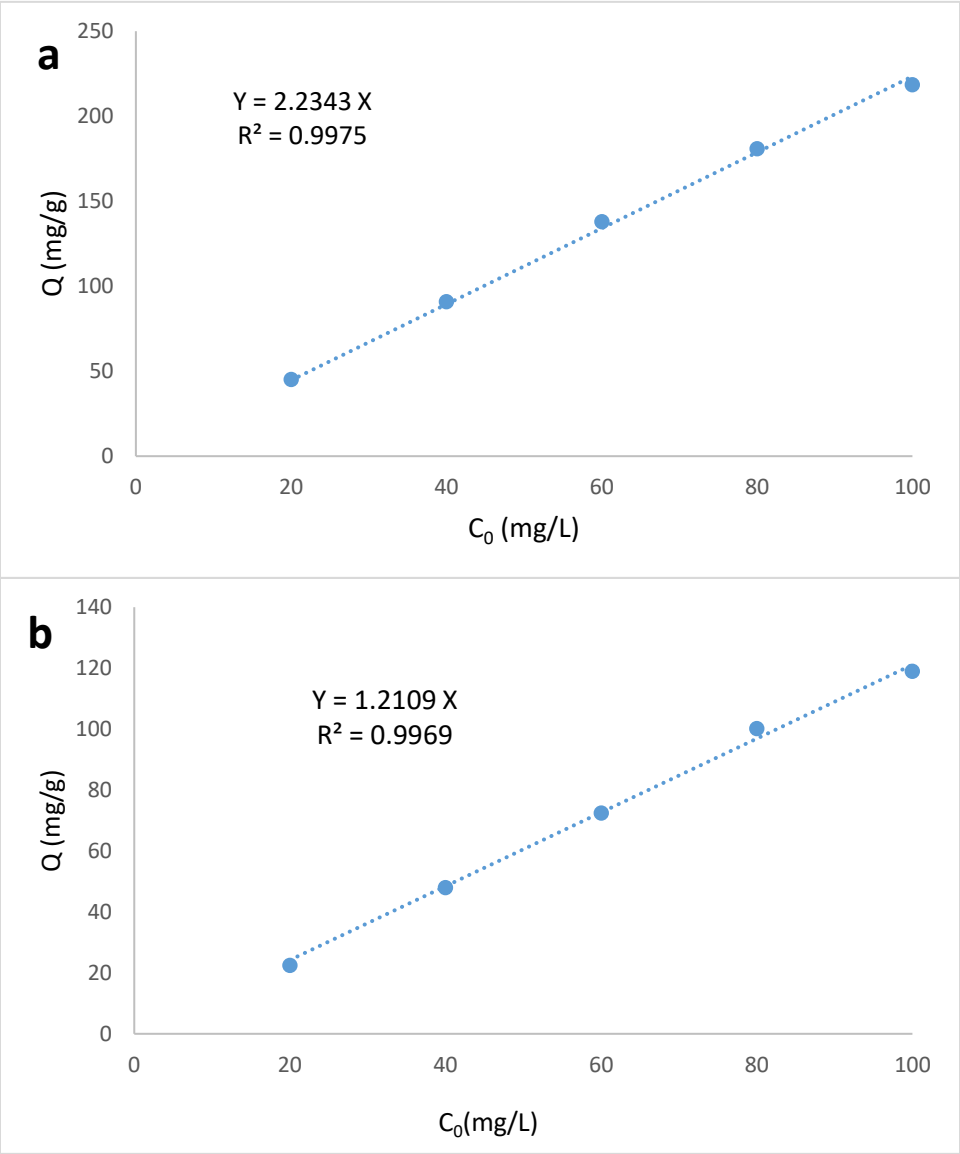

Figure 3.22 Variation of Q with C_0 for BPB removal by: (a) Fe NPs, (b) Fe-Ni NPs at 323 K

Table 3.9 gives the values of ΔH°, ΔG° and ΔS° associated with the removal of BPB at different initial concentrations of 20, 40, 60, 80 and 100 mg/L, at two temperatures; 298 and 323K.

The enthalpy values are negative for BPB removal by both of Fe and Fe-Ni, indicating exothermic behavior. In both cases, negative entropy changes of the system are obtained, indicating the dye sorption yields more order in the system. The negative standard Gibbs energy changes show that the reaction distinctly favors the products over the reactants. The exothermic behavior and negative entropy changes are usually associated when the solute has relatively low hydration energies; i.e the solute has high chemical potential in the solution. Thus, the fixation of the solute on the solid surface will be driven by intrinsic enthalpy changes (negative), with small contribution from enthalpy of dehydration (positive), such that the resultant enthalpy change is negative. This process is associated with increasing order in the system, yielding a negative entropy change.

Being a charge less molecule with a relatively large molecular size, BPB is not expected to have strong solvation energies in water, as it is the case with charged and small molecules.[78]

Table 3.9 The values of ΔH°, ΔG° and ΔS° associated with removal of BPB from solutions at temperatures of 298 and 323K.

		298 K		323 K	
Sample	**ΔH°(kJ/mol)**	**ΔG°(kJ/mol)**	**ΔS°(J/mol.K)**	**ΔG° (kJ/mol)**	**ΔS°(J/mol.K)**
Fe	-35.8	-27.4	-28.2	-26.7	-28.2
Fe-Ni	-51.9	-23.2	-96.3	-20.8	-96.3

3.6 Effect of pH on the Removal of BPB

The effect of pH on the removal of BPB by Fe and Fe-Ni NPs was investigated using a buffer system adjusted at values of 4.0, 6.0 and 8.0. The removal process was very active at pH 4 and inactive at the other pH values. The dye is an acid dye which is effective at low pH values. On the other hand, it is reported that low pH values cause enhancement in nZVI reactivity, which is induced by the acceleration of iron corrosion and dissolution of the passivated layers on the nZVI surface. At high pH values, nZVI reactivity is lowered due to the precipitation of ferrous hydroxide on the nZVI surfaces, leading to the inhibition of electron transfer from the Fe(0) core to the outermost oxide surface. [79]

3.7 Degradation Products Analysis

The U-Vis spectra of BPB solutions after the removal process showed the disappearance of the dye peak at 590 nm and the dye broad peak at 440 nm, and the appearance of a new shoulder peak at 317 nm. Figure 3.23 provides two typical spectra.

This result could be considered as an indication of the degradation of the BPB during the removal process by nanoparticles materials. This topic and the identification of the degradation products can be the subject of a future study.

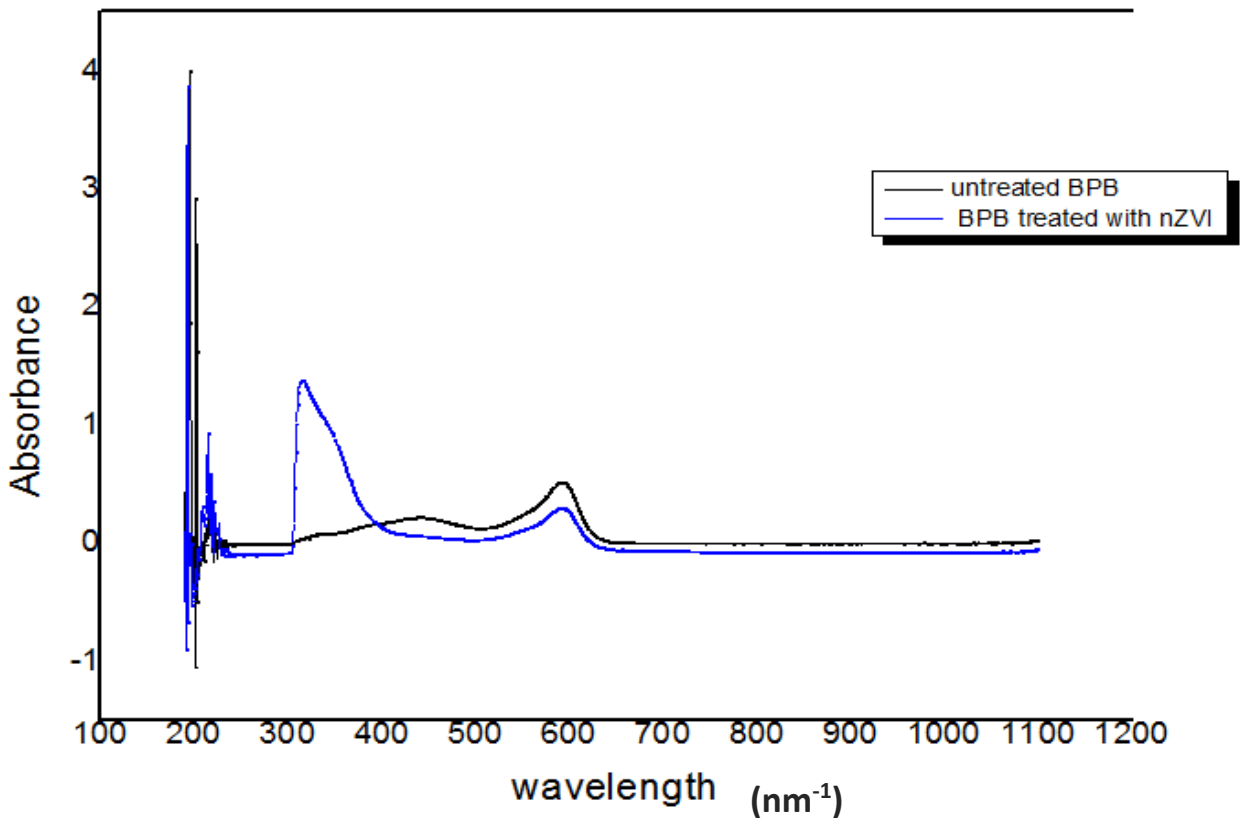

Figure 3.23 UV-Vis spectra of BPB before and after treatment with Fe NPs.

4. Conclusions

Iron nanoparticles (Fe NPs) and iron nickel bimetallic nanoparticles (Fe-Ni NPs) can readily be prepared by liquid phase reduction using sodium borohydride as a reducing agent. Fe-Ni NPs were observed to be smaller than Fe NPs, but the extent of aggregation is seen to be larger in Fe-Ni NPs. Both of the materials possess chain-like morphology, which limit their dispersion in aqueous solution. Future work can focus on synthesizing the material (in particular Fe-Ni NPs) in the presence of a support material in order to enhance their dispersion.

Comparing the efficiency of Fe and Fe-Ni NPs in removing bromophenol blue dye from water, the following conclusions can summerized:

- On the overall, the efficiency of bromophenol blue removal efficiency using Fe NPs was higher than that by using Fe-Ni NPs. It is observed that, as the nickel percentage increases the efficiency decreases.
- The Fe NPs take shorter time to remove BPB from water compared with Fe-Ni NPs, and the process can be described by pseudo second order kinetics.
- For both types of NPs, the extent of removal decreased as the temperature increased, indicating exothermic behavior.

- Apparent equilibrium constants were calculated over the concentration range (20-100) mg/L using a modified form of the linear isotherm, in which the initial concentration is the dependent variable.

Future studies are needed to investigate the degradation products of the reaction. In addition, further experiments can be done on Fe-Ni NPs using Fenton catalyst.

5. References

(1) Yunus, I. S.; Kurniawan, A.; Adityawarman, D.; Sofian, I.; Kurniawan, A.; Adityawarman, D. Nanotechnologies in Water and Air Pollution Treatment.*Environ. Technol.* **2012**, *1*(1), 136-148.

(2) Alrumman, S. A.; El-kott, A. F.; Keshk, S. M. A. S. Water Pollution : Source and Treatment. *Am. J. Environ. Eng.* **2016**, *6*(3),88-98.

(3) Alvarez, P. J. J. Nanotechnology for a Safe and Sustainable Water Supply : Enabling Integrated Water Treatment and Reuse. *Acc. Chem. Res.*. **2012**.

(4) Qu, X.; Alvarez, P. J. J.; Li, Q. Applications of Nanotechnology in Water and Wastewater Treatment. *Water Res.* **2017**, *47* (12), 3931–3946.

(5) Brame, J.; Li, Q.; Alvarez, P. J. J. Nanotechnology- Enabled Water Treatment and Reuse : Emerging Opportunities and Challenges for Developing Countries. *Trends Food Sci. Technol.* **2011**, *22* (11), 618–624.

(6) Shannon, M. A.; Bohn, P. W.; Elimelech, M.; Georgiadis, J. G.; Marin, B. J.; Mayes, A. M. Science and Technology for Water Purification in the Coming Decades. *Nature.* **2008**, *452*, 301–310.

(7) Vysokomornaya, O. V; Balakhnina, J. E.; Shikhman, M. V. Thermal Treatment of Industrial Wastewater. *EDP Sci.* **2015**, *5*, 10–13.

(8) Padhi, B. S. Pollution Due to Synthetic Dyes Toxicity & Carcinogenicity Studies and Remediation. *Environ. Sci.* **2012**, *3* (3), 940–955.

(9) Agustiono, T.; Chan, G. Y. S.; Lo, W.; Babel, S. Physico – Chemical Treatment Techniques for Wastewater Laden with Heavy Metals. *Chem. Eng. J.* **2006**, *118*, 83–98.

(10) Kabbout, R.; Taha, S. Biodecolorization of Textile Dye Effluent by Biosorption on Fungal Biomass Materials. *Phys. Procedia* . **2014**, *55*, 437–444.

(11) Kaushik, P.; Malik, A. Fungal Dye Decolourization : Recent Advances and Future Potential. *Environ. Int.* **2009**, *35* (1), 127–141.

(12) Sharma, Y. C.; Srivastava, V.; Singh, V. K.; Kaul, S. N.; Weng, C. H. Nano - Adsorbents for the Removal of Metallic Pollutants from Water and Wastewater. *Environ. Technol*. **2009**, 30(6), 583-609.

(13) Crane, R. A.; Scott, T. B. Nanoscale Zero-Valent Iron : Future Prospects for an Emerging Water Treatment Technology. *J. Hazard. Mater.* **2012**, *212(211)*, 112–125.

(14) Bhattacharya, S.; Saha, I.; Mukhopadhyay, A; Chattopadyay, D.; Ghosh,U.C.; Chatterjee,D. Role of Nanotechnology in Water Treatment and Purification : Potential Applications and Implications. *Int. J. Chem. Sci. Technol.* **2014**, *3*(3),59-64.

(15) Elliott, D. W.; Li, X.; Elliott, D. W.; Zhang, W. Zero-Valent Iron Nanoparticles for Abatement of Environmental Pollutants : Materials and Engineering Aspects. *Crit. Rev. Solid State Mater. Sci.* **2006**, *3*, 111-122.

(16) Chokshi, N.; Bora, L. An Overview of Nanotechnology in WasteWater Treatment. **2014**.conference paper. Conference: Resource recovery, water reuse and recycle for sustainable development At: G. H. Patel Engineering College, Ananad.

(17) Theron, J.; Walker, J. A.; Cloete, T. E. Nanotechnology and Water Treatment : Applications and Emerging Opportunities. *Crit. Rev. microbiol.* **2008**, *34*, 43–69.

(18) Li, X.; Zhang, W. Iron Nanoparticles : The Core - Shell Structure and Unique Properties for Ni (II) Sequestration. *Langmiur.* **2006**, 22(10), 4638–4642.

(19) Bystrzejewska-piotrowska, G.; Golimowski, J.; Urban, P. L. Nanoparticles : Their Potential Toxicity , Waste and Environmental Management. *Waste Manage.* **2009**, *29* (9), 2587–2595.

(20) Castañeda, R.; León, S.; Robles-belmont, E.; Záyago, E. Review of Nanotechnology Value Chain for Water Treatment Applications In Mexico. *Resour. Technol.* **2017**.

(21) Zhang, Y.; Chen, W.; Dai, C.; Zhou, C.; Zhou, X. Structural Evolution of Nanoscale Zero-Valent Iron (nZVI) in Anoxic Co^{2+} Solution : Interactional Performance and Mechanism. *Sci. Rep.* **2015**,*5*.

(22) Bae, S.; Hanna, K.; Nationale, E. Reactivity of Nanoscale Zero-Valent Iron in Unbuffered Systems: Effect of PH and Fe(II) Dissolution. *Environ. Sci. Technol.* **2015**.

(23) Thiruvenkatachari, R.; Vigneswaran, S.; Naidu, R. Permeable Reactive Barrier for Groundwater Remediation. *Ind. Eng. Chem. Res.* **2008**, *14*, 145–156.

(24) Toshima, N.; Yonezawa, T. Bimetallic Nanoparticles Novel Materials for Chemical and Physical Applications . *New J. Chem.* **1998**, 1179–1201.

(25) Zhang, W.; Wang, C.; Lien, H. Treatment of Chlorinated Organic Contaminants with Nanoscale Bimetallic Particles. *Catal. Today.* **1998**, *40*, 387-395.

(26) Gunawardana, B.; Singhal, N.; Swedlund, P. Degradation of Chlorinated Phenols by Zero Valent Iron and Bimetals of Iron : A Review. *Environ. Eng. Res.* **2011**, *16* (4), 187–203.

(27) Cheng, S.; Wu, S. The Enhancement Methods for the Degradation of TCE by Zero-Valent Metals. *Chemoshpere.* **2000**, *41*. 1263-1270.

(28) Cheng, S.; Wu, S. Feasibility of Using Metals to Remediate Water Containing TCE. *Chemoshpere.* **2001**, *43*, 1023-1028.

(29) Schrick, B.; Blough, J. L.; Jones, A. D.; Mallouk, T. E. Hydrodechlorination of Trichloroethylene to Hydrocarbons Using Bimetallic Nickel-Iron Nanoparticles. *Chem. Mater.* **2002**, *14* (12), 5140–5147.

(30) Science, E.; Britain, G. Research Note a Method For The Rapid Dechlorination Of Low Molecular Weight Chlorinated Hydrocarbons In Water. *Wat. Res.* **1995**, *29* (10), 2434–2439.

(31) Wang, C. B.; Zhang, W. X. Synthesizing Nanoscale Iron Particles for Rapid and Complete Dechlorination of TCE and PCBs. *Environ. Sci. Technol.* **1997**, *31* (7), 2154–2156.

(32) Tee, Y; Bachas,L; Bhattacharyya, D. Degradation of Trichloroethylecne and Dichlorobiphenyls by Iron-Based Bimetallic Nanoparticles. *J. Phys. Chem. C*. **2009**, *113* (22), 9454–9464.

(33) Savage, N.; Diallo, M. S. Nanomaterials and Water Purification : Opportunities and Challenges. *J. Nanopart. Res.* **2005**, 7,331-342.

(34) Smuleac, V.; Varma, R.; Sikdar, S.; Bhattacharyya, D. Green Synthesis of Fe and Fe/Pd Bimetallic Nanoparticles in Membranes for Reductive Degradation of Chlorinated Organics. *J. Memb. Sci.* **2011**, *379*(1-2), 131–137.

(35) Xu, J.; Bhattacharyya, D. Membrane Based Bimetallic Nanoparticles for Environmental Remediation : Synthesis and Reactive Properties. *Environ. Prog.* **2005**, *24* (4).

(36) Arnold, W. A.; Burris, D. R.; Campbell, T. J. Reductive Elimination of Chlorinated Ethylenes by Zero-Valent Metals. *Environ. Sci. Technol.* **1996**, *30* (8), 2654–2659.

(37) Gotpagar, J.; Lyuksyutov, S.; Cohn, R.; Grulke, E.; Bhattacharyya, D. Reductive Dehalogenation of Trichloroethylene with Zero-Valent Iron : Surface Profiling Microscopy and Rate Enhancement Studies. *Langmuir*. **1999**, 15, 8412–8420.

(38) Chen, J.; Al-abed, S. R.; Ryan, J. A.; Li, Z. Effects of PH on Dechlorination of Trichloroethylene by Zero-Valent Iron. *J. Hazard. Mater.* **2001**, *83*, 243–254.

(39) Zhu, N.; Luan, H.; Yuan, S.; Chen, J.; Wu, X.; Wang, L. Effective Dechlorination of HCB by Nanoscale Cu / Fe Particles. *J. Hazard. Mater.* **2010**, *176*, 1101–1105.

(40) Vijayakumar, N. S.; Flower, N. A. L.; Brabu, B.; Raja, S. V. K. Degradation of DCE and TCE by Fe – Ni Nanoparticles Immobilised Polysulphone Matrix. *J. Exp. Nanosci*. **2013**, *8*(7-8), 890-900,

(41) Zhu, B.; Lim, T. Catalytic Reduction of Chlorobenzenes with Pd / Fe Nanoparticles : Reactive Sites , Catalyst Stability , Particle Aging , and Regeneration.*Environ. Sci. Technol*. **2007**, *41* (21), 7523–7529.

(42) Wu, L.; Ritchie, S. M. C. Removal of Trichloroethylene from Water by Cellulose Acetate Supported Bimetallic Ni / Fe Nanoparticles. *Chemosphere*. **2006**, *63*, 285–292.

(43) Odziemkowski, M. S.; Gui, L. A. I.; Gillham, R. W. Reduction of N - Nitrosodimethylamine with Granular Iron and Nickel-Enhanced Iron . 2 . Mechanistic Studies. *Environ. Sci. Technol.* **2000**, *34* (16), 3495–3500.

(44) Bokare, A. D.; Chikate, R. C.; Rode, C. V; Paknikar, K. M. Iron-Nickel Bimetallic Nanoparticles for Reductive Degradation of Azo Dye Orange G in Aqueous Solution. *Appl. Catal., B.* **2008**, *79*, 270–278.

(45) Meyer, D. E.; Wood, K.; Bachas, L. G.; Bhattacharyya, D. Degradation of Chlorinated Organics by Membrane-Immobilized Nanosized Metals. *Environ. Prog.***2004**, *23* (3).

(46) Tee, Y.; Grulke, E.; Bhattacharyya, D. Role of Ni / Fe Nanoparticle Composition on the Degradation of Trichloroethylene from Water. *Ind. Eng. Chem. Res.* **2005**, *44* ,*7062*–7070.

(47) Mehari, A. K.; Gebremedhin, S.; Ayele, B. Effects of Bahir Dar Textile Factory Effluents on the Water Quality of the Head Waters of Blue Nile River , Ethiopia. *Int. J. Anal. Chem.*. **2015**.

(48) Oros, G.; Forgacs, E.; Cserha, T. Removal of Synthetic Dyes from Wastewaters : A Review. *Environ. Int.* **2004**, *30*, 953–971.

(49) Arora, S. Textile Dyes : It ' s Impact on Environment and Its Treatment. *J. Bioremed. Biodeg.* **2014**, *5* (3), 6199.

(50) Maria, F.; Chequer, D.; Augusto, G.; Oliveira, R. De; Raquel, E.; Ferraz, A.; Cardoso, J. C. Eco-Friendly Textile Dyeing and Finishing. Melih Gunay(Ed). InTech; Shanghai, China **2013**

(51) Jaganathan, V.; Busi, I.; Mgt, M. P.; Int, M. P.; Mba, B.; Premapriya, M. S.; Phil, M. Environmental Pollution Risk Analysis And Management In Textile Industry : A Preventive Mechanism. *Eur. Sci. J.* **2014**, *2*, 1857 – 7881.

(52) S, D. N. Pollution Effects & Control Impact of Dyeing Industry Effluent on Groundwater Quality by Water Quality Index and Correlation Analysis. *J. Pollut. Eff. Cont*. **2014**, *2* (2), 2–5.

(53) Akarslan, F.; Demiralay, H. Effects of Textile Materials Harmful to Human Health. *Acta Phys. Pol., A*. **2015**, *128* (2), 407–408.

(54) Sivakumar, P.; Palanisamy, P. N. Low-Cost Non-Conventional Activated Carbon For The Removal Of Reactive Red 4 : Kinetic And Isotherm Studies. *Rasayan J. Chem.* **2008**, *1*(4),871-883.

(55) Ong, S.; Keng, P.; Lee, W.; Ha, S.; Hung, Y. Dye Waste Treatment. *Water.* **2011**, *7* (3), 157–176.

(56) Claxton, L. D.; Houk, V. S.; Hughes, T. J. Genotoxicity of Industrial Wastes and Effluents. *Mutat. Res*.**1998**, 410,237–243.

(57) Huber, D. L. Reviews Synthesis , Properties , and Applications of Iron Nanoparticles. *Small.* **2005**, *1*(5), 482–501.

(58) Azmat, R.; Khalid, Z.; Haroon, M.; Perveen, K. Spectral Analysis of Catalytic Oxidation and Degradation of Bromophenol Blue at Low pH With Potassium Dichromate. *Adv. Nat. Sci.* **2013**, *6* (3), 38–43.

(59) Iqbal, M. J.; Ashiq, M. N. Adsorption of Dyes from Aqueous Solutions on Activated Charcoal. *J. Hazard. Mater*. **2007**, *139*, 57–66.

(60) Dhananasekaran, S.; Palanivel, R. Adsorption of Methylene Blue , Bromophenol Blue , and Coomassie Brilliant Blue by a -Chitin Nanoparticles. *J. Adv. Res.* **2016**, *7* (1), 113–124.

(61) El-zahhar, A. A.; Awwad, N. S.; El-katori, E. E. Removal of Bromophenol Blue Dye from Industrial Waste Water by Synthesizing Polymer-Clay Composite. *J. Mol. Liq.* **2014**, *199*, 454–461.

(62) Bouanimba, N.; Zouaghi, R.; Laid, N.; Sehili, T. Factors in Fl Uencing the Photocatalytic Decolorization of Bromophenol Blue in Aqueous Solution with Different Types of TiO_2 as Photocatalysts. *Desalination*.**2011**, *275* (1–3), 224–230.

(63) Mohammadzadeh, A.; Ramezani, M.; Ghaedi, A. M. Using Ultrasonic Assisted Method : Optimization by Response Surface Methodology and Genetic Algorithm. *J. Taiwan Inst. Chem. Eng.* **2015**, 1–10.

(64) Alireza, Q.; Zabihi-mobarakeh, H. Journal of Industrial and Engineering Chemistry Heterogeneous Photodecolorization of Mixture of Methylene Blue and Bromophenol Blue Using CuO-Nano-Clinoptilolite. *J. Ind. Eng. Chem.* **2013**, 1–11.

(65) Karabelli, D.; Ünal, S.; Shahwan, T.; Eroĝlu, A. E. Preparation and Characterization of Alumina-Supported Iron Nanoparticles and Its Application for the Removal of Aqueous Cu^{2+} Ions. *Chem. Eng. J.* **2011**, *168* (2), 979–984.

(66) Sun, Y.; Li, X.; Cao, J.; Zhang,W.; Wang, P. Characterization of zero-valent iron nanoparticles. *Adv. Colloid Interface Sci.* **2006**.120, 47–56.

(67) Fuchs, H.; Nairat, M.; Shahwan, T.; Erog, A. E. Incorporation of Iron Nanoparticles into Clinoptilolite and Its Application for the Removal of Cationic and Anionic Dyes. *J. Ind. Eng. Chem.* **2015**, *21*, 1143–1151.

(68) Çelebi, O.; Üzüm, Ç.; Shahwan, T.; Erten, H. N. A Radiotracer Study of the Adsorption Behavior of Aqueous Ba^{2+} Ions on Nanoparticles of Zero-Valent Iron. *J. Hazard. Mater.* **2007**, *148*, 761–767.

(69) Üzüm, Ç.; Shahwan, T.; Eroğu, A. E.; Lieberwirth, I.; Scott, T.B.; Hallam, K.R. Application of Zero-Valent Iron Nanoparticles for the Removal of Aqueous Co^{2+} Ions under Various Experimental Conditions. *Chem. Eng. J.* **2008**, *144*, 213–220.

(70) Liu, A.; Liu, J.; Zhang, W. Transformation and composition evolution of nanoscale zero valent iron (nZVI) synthesized by borohydride reduction in static water. *Chemosphere*. **2015**, 119, 1068–1074.

(71) Grosvenor, A. P.; Kobe, B. A.; Biesinger, M. C.; McIntyre, N. S. Investigation of Multiplet Splitting of Fe 2p XPS Spectra and Bonding in Iron Compounds. *Surf. Interface Anal.* **2004**, *36* (12), 1564–1574.

(72) Chandra, S.; Kumar, A.; Tomar, P. K. Synthesis of Ni Nanoparticles and Their Characterizations. *J. Saudi. Chem. Soc.* **2014**, *18* (5), 437–442.

(73) Biesinger, M. C.; Payne, B. P.; Grosvenor, A. P.; Lau, L. W. M.; Gerson, A. R.; St, R.; Smart, C. Applied Surface Science Resolving Surface Chemical States in XPS Analysis of First Row Transition Metals , Oxides and Hydroxides : Cr , Mn , Fe , Co and Ni. *Appl. Surf. Sci.* **2011**, *257* (7), 2717–2730.

(74) Wu, W.; He, Q.; Jiang, C. Magnetic Iron Oxide Nanoparticles : Synthesis and Surface Functionalization Strategies. *Nanoscale Res. Lett.* **2008**,*3*, 397–415.

(75) Shahwan, T. Lagergren Equation: Can Maximum Loading of Sorption Replace Equilibrium Loading? *Chem. Eng. Res. Des.* **2015**, *96*, 172–176.

(76) Oboh, I. O.; Aluyor, E. O.; Audu, T. O. K. Second-Order Kinetic Model for the Adsorption of Divalent Metal Ions on Sida Acuta Leaves. *Int. J. Phys. Sci.* **2013**, *8* (34), 1722–1728.

(77) Shahwan, T. Author ' s Personal Copy Sorption Kinetics : Obtaining a Pseudo-Second Order Rate Equation Based on a Mass Balance Approach. *J. Environ. Chem. Eng.* **2014**, *2*, 1001‑1006.

(78) Anayana Z. Dangui, Vanessa M.S. Santos, Benhur S. Gomes,Taiane S. de Castilho, Keller P. Nicolini, Jaqueline Nicolini. Preferential Solvation Bromophenol Blue in Water-Alcohol Binary Mixture. *Mol. Biomol. Spectrosc.* **2017**.

(79) Bae, S.; Hanna, K. Reactivity of Nanoscale Zero-Valent Iron in Unbuffered Systems: Effect of PH and Fe(II) Dissolution. *Environ. Sci. Technol.* **2015**, *49* (17), 10536–10543.

(80) Wu, S.H.; Chen, D.H. Synthesis and characterization of nickel nanoparticles by hydrazine reduction in ethylene glycol. *J. Colloid Interface Sci.* **2003**, *259*, 282–286.

(81) Chen, D.H.; Hsieh, C.H. Synthesis of nickel nanoparticles in aqueous cationic surfactant solutions. *J. Mater. Chem.* **2002**, *12*, 2412–2415.